To the Graduate Council:

I am submitting herewith a thesis written by Nadine Lynelle Lashier entitled "Use of Shuttle Orbiter Aerodynamic Data to Validate Accommodation Coefficient Models." I have examined the final copy of this thesis for form and content and recommend that it be accepted in partial fulfillment of the requirements for the degree of Master of Science, with a major in Aerospace Engineering.

Frank Collins, Major Professor

We have read this thesis and recommend its acceptance:

Accepted for the Council:

Associate Vice Chancellor and
Dean of The Graduate School

USE OF SHUTTLE ORBITER AERODYNAMIC DATA TO VALIDATE ACCOMMODATION COEFFICIENT MODELS

A Thesis
Presented for the Master of Science
Degree
The University of Tennessee, Knoxville

Nadine Lynelle Lashier
May 1999

DEDICATION

This thesis is dedicated to my parents,

Larry and Charlene Lashier,

who always support me

in whatever I do.

ACKNOWLEDGMENTS

I would like to thank Dr. Frank Collins, my advisor and chairman of my committee, for his guidance during the writing of this thesis. Also, I would like to thank the members of my committee, Dr. Gary Flandro and Dr. Bill Lewis, for their advice and guidance. There are several other people I would like to acknowledge: Peter Demerest, former UTSI student, for his assistance in providing background information, Dr. Robert Blanchard of NASA Langley Research Center for providing information on the Space Shuttle, and David Adamczak at Wright Patterson for providing the VECC Program. Without the assistance of all these people, this thesis would never have been completed.

ABSTRACT

Knowledge of the free-molecule flow regime is important in order to determine precise satellite orbits and to find the bridging function between continuum flow and free-molecule flow for use in the development of single-stage-to-orbit vehicles. For this thesis, two variable accommodation coefficient models were integrated into the computer program used to calculate the aerodynamic forces present on a body, and the results were compared with measured values from the Space Shuttle Orbiter. It was concluded that although the diffuse method under-predicts the aerodynamic lift present on the Orbiter in low-earth orbit, the variable accommodation coefficient models vastly over-predict the amount of lift present. This difference is attributed to the fact that the tiles on the Orbiter are non-engineering surfaces. Also, unlike predictions using the variable models, lift-to-drag ratio predictions using the diffuse model were very sensitive to wall temperature and atmospheric temperature and composition. It is recommended that experiments be performed in orbit, coupled with direct measurements of atmospheric conditions, to produce real data that could be used to improve the mathematical models.

Ref' MAY 04 '01

TABLE OF CONTENTS

CHAPTER PAGE

1. INTRODUCTION 1

2. BACKGROUND 5
   2.1 Free-molecule Flow 5
   2.2 Previous Work 11
   2.3 Viscous Effects on Complex Configurations Computer Code 19
   2.4 The Space Shuttle Orbiter 20

3. CALCULATIONS 23
   3.1 Lift-to-drag Ratio 23
   3.2 Experimental Measurements 24
   3.3 Input Parameters/Conditions 26
   3.4 Assumptions 27

4. RESULTS 31
   4.1 Results of Calculations 31
   4.2 Sensitivity Tests 33

5. CONCLUSIONS 39

6. RECOMMENDATIONS 41

REFERENCES 43

APPENDICES 47

APPENDIX A: THE VISCOUS EFFECTS ON COMPLEX CONFIGURATIONS COMPUTER CODE 48
   A.1 Running Viscous Effects on Complex Configurations 49
   A.2 Using Viscous Effects on Complex Configurations 51

APPENDIX B: VECC MAKEFILES 54
   B.1 Main Program Makefile 55
   B.2 Gui Makefile 56
   B.3 Mk5 Makefile 58
   B.4 PrepMk5 Makefile 65

CHAPTER PAGE

B.5 Plot Makefile 67
B.6 Trim Makefile 68

APPENDIX C: SPACE SHUTTLE ORBITER CENTER OF GRAVITY LOCATIONS 69

APPENDIX D: STANDARD ATMOSPHERIC PROPERTIES 78

VITA 80

LIST OF TABLES

TABLE PAGE

1. Space Shuttle Orbiter Centers of Gravity 22

2. Calculated Aerodynamic Coefficients 32

3. Normalized Calculated Aerodynamic Coefficients 32

4. Effects of Vaying Temperature Ratio 34

5. Effects of Varying Speed Ratio 36

6. Effects of Varying Angle of Attack 37

7. Detailed Space Shuttle Orbiter Center of Gravity Locations 70

LIST OF FIGURES

FIGURE PAGE

1. Coordinate System for Gas-Surface Interaction 10
2. Momentum Accommodation Coefficient Measurements 14
3. Momentum Accommodation Coefficients Given by Models 15 and 17..... 15
4. The European Remote Sensing Satellite (ERS-1). 16
5. Geometric Model of the ERS-1 Satellite..... 17
6. Aerodynamic Coefficients for the ERS-1 Satellite..... 18
7. Geometric Model of the Space Shuttle Orbiter 21
8. Measured Lift-to-drag Ratio for the Space Shuttle Orbiter 26
9. Velocity/Altitude Parameters for Several Re-entry Vehicles 30
10. Comparison of Calculations and Measured Lift-to-drag Ratios..... 34
11. Solar Cycle Activity 38

LIST OF SYMBOLS

C_D	Coefficient of drag
C_f	Shear coefficient
C_L	Coefficient of lift
C_P	Pressure coefficient
D	Drag
Kn	Knudsen Number
L	Lift
L_b	Typical/characteristic body dimension
M	Mach Number
P	Normal momentum
R	Gas constant
R_a	Ratio of measured accelerations
S	Speed ratio
T_{inf}	Free stream temperature
T_w	Temperature at the body surface
V	Speed of the body
cg	Subscript meaning the center of gravity
f	Maxwell's fraction
i	Subscript referring to incident characteristics

r	Subscript referring to re-emitted characteristics
w	Subscript that denotes conditions on the wall surface
α	Angle of attack
δ	Angle between velocity and surface tangent
γ	Specific heat ratio
λ	Mean free path
θ	Angle between velocity and surface normal
σ'	Normal accommodation coefficient
σ	Tangential accommodation coefficient
τ	Tangential momentum

CHAPTER 1: INTRODUCTION

Contrary to what most people believe, the science of an orbiting satellite is not perfectly understood. As more and more satellites are being launched into low-earth orbit and NASA is looking at the next generation of launch vehicles, a better understanding of bodies in orbital conditions is vital. There are two basic reasons that scientists are interested in obtaining good information on the orbital environment: determining precise satellite orbits and finding the bridging relation between continuum and free-molecule flow for single-stage-to-orbit vehicles.

Two recent events show just how important a good understanding of orbital conditions is. For a long time, scientists have been unable to explain why satellites observe a cooling trend in the troposphere while ground stations have observed warming trends and climate models show warming both on the ground and in the troposphere. Recently, however, two scientists discovered a problem in the satellite data analysis that calculates the temperature of the atmosphere. Apparently, the satellite orbit decay was not taken into account. Once the satellite orbit was corrected, data from the satellite agreed with the other measured data (Hansen et al., 1998). During the first Space Shuttle flight, the body flap deflection necessary to maintain the desired trim was 100 percent larger than expected. Fortunately, the flaps had large enough margins to satisfy the need, allowing the Shuttle to land safely (Knox, Collins and Liver, 1991). Both of these situations could have been avoided with a better understanding of the low-earth orbit environment.

Current methods used to calculate satellite orbits and the amount of lift and drag present on satellites and space vehicles use accommodation coefficient models in the calculations. In low earth orbit, the forces present on a satellite are all of comparable magnitude. The forces are on the order of 10^{-5} Newton, and all have a high level of uncertainty. It is difficult to measure forces and accelerations of this size, and the measurements that have been made are very uncertain. Traditionally, evaluations of the forces on satellites have neglected any lift present on the satellite, assuming that there was none, or what lift there was had little or no effect. However, recent studies have shown that there is lift acting on the satellite. If this is the case, yet another uncertainty is added to already questionable results. To eliminate some of these uncertainties, we need accurate estimates of the lift, drag, moment, and other forces acting on a satellite in orbit. More accurate accommodation coefficient models would be part of the solution to the problem.

In developing Single-Stage-to-Orbit (SSTO) vehicles, the heating of the spacecraft is very important. We want to maximize the payload fraction (amount of payload a spacecraft can deliver to orbit compared to the amount of fuel required to reach orbit) while minimizing the fuel required. To accomplish these goals, the aerodynamic properties of the vehicle in all the flow regimes must be known. This data forms a "bridging function" anchored at each end by known flow conditions. The behavior of fluids in the continuum region is understood, but much is still not known about the free-molecule (or rarefied) flow region. Free-molecule flow aerodynamics are a function of accommodation coefficients. More accurate

accommodation coefficient models could greatly improve our understanding of the free-molecule regime, which would help define the bridging function, eventually making the single-stage-to-orbit vehicle a reality.

To correctly reproduce orbital conditions, data is needed for atmospheric molecules in their ground state at 5 – 15 eV relative energy colliding with "engineering surfaces," which are polycrystalline and contain adsorbed gases. These are conditions that have not been reproduced in the laboratory. Some data does exist, but it is principally for ions accelerated to this energy range. Frank Collins from the University of Tennessee Space Institute examined all of the data that is in any way related and generated curve fits to the data. All of these data indicate lobular scattering patterns rather than the circular scattering patterns suggested by the traditional diffuse model. A study by Peter Demerest (1996) used one of these curve fits to show that the orbital prediction of one satellite with very large solar panels was improved relative to the orbital prediction using the traditional diffuse model. This improvement was thought to be due to the prediction of increased lift by the new accommodation coefficient curve fit that was used.

The purpose of this thesis was to improve the aerodynamic prediction for the Space Shuttle Orbiter by using two particular accommodation coefficient models. The models were integrated into an existing computer program used to calculate the aerodynamic lift and drag for the Orbiter, and the calculated results were then compared with the measured values. Also, tests were done to check the

sensitivity of the accommodation coefficient models to various physical factors such as wall temperature, speed, and angle of attack. It was not the purpose of this study to validate a particular accommodation coefficient model or prove the existing data incorrect. Instead, the need for more aerodynamic measurements under orbital conditions is shown.

CHAPTER 2: BACKGROUND

2.1 Free-molecule Flow

At high altitudes, the density of the atmosphere is so low that the molecules reflected from the surface of the vehicle have no effect on the incoming molecules, and the incoming and reflected momentum streams are basically independent of each other. This region is defined as free-molecule flow (Collins and Knox, 1995). Free-molecule (rarefied) flow is different from continuum flow in four basic ways. First, rarefied flow has no boundary layer or shock wave formed on the surface of the body. Second, in free-molecule flow, the aerodynamic forces are a direct result of momentum transfers between the atmosphere particles and the body. Third, incident and reflected particles have no influence on each other, i.e. there are no secondary collisions to worry about. Fourth, the free-stream molecules have a Maxwellian distribution of thermal velocity superimposed on their bulk velocity, which is true because the atmosphere as a whole is in thermal equilibrium (Crowther and Stark, 1991).

As the atmospheric density increases, collisions begin to occur between incoming and reflected molecules, and the momentum streams are no longer independent. This region is called the transition regime, where the flow cannot be defined as strictly continuum flow or strictly free-molecule flow. In order to make any sense of the behavior of satellites in low-earth orbit, an understanding of free-molecule flow and transition flow is vital.

Knudsen Number

The Knudsen number is the dimensionless quantity used to define what type of fluid flow is present around a body. It is defined as

$$Kn = \frac{\lambda}{L}, \qquad [1]$$

where λ is the mean free path (average distance between collisions) of the molecules in the atmosphere, and L is the characteristic length (typically the length of a satellite or the cord of a winged body) of the body in question. Generally, if Kn <<1, the body is in standard continuum flow. If Kn > 50, the body is in free-molecule flow. If the Knudsen number is between 0.1 and 50, the body is in transition flow, which is a combination of the two regimes (Moore and Sowter, 1991).

The speed ratio is a dimensionless number used to determine whether or not a fluid flow is hyperthermal. It is defined as the ratio of the vehicle speed to the most probable random speed of the atmospheric molecules (Collins and Knox, 1995). A high speed ratio indicates that the flow is hyperthermal, which in turn means that the random velocity given by the Maxwellian velocity distribution can be ignored. However, this is rarely the case in the atmosphere since the temperatures are so high. The speed ratio is defined as

$$S = \frac{V}{\sqrt{2RT}} = M\sqrt{\frac{\gamma}{2}}, \qquad [2]$$

where S is the speed ratio, V is the velocity of the body, R is the gas constant, T is the gas temperature, and γ is the specific heat ratio (Demerest, 1996). The second

part of Equation [2] is misleading, as the Mach number has no significance in rarefied flow since there are no sound waves. Also, in rarefied flow, only the heat transfer is dependent on the specific heat ratio. The only reason to include the second part of the equation is that the computer codes currently used to calculate lift and drag require the Mach Number as an input quantity. For a general satellite in low-earth orbit, the speed ratio ranges from 8 to 15.

Accommodation Coefficients

In the late 1870s, Maxwell developed the idea that a fraction (f) of the incident molecules would adhere to the surface of a body long enough to come to thermal equilibrium with the surface and would then be reflected from the surface in a diffuse manner. The rest of the molecules ($1 - f$) would be reflected specularly. This assumption is still used today even though it does not accurately describe the gas/surface interactions and results in inaccurate aerodynamic force predictions (Collins and Knox, *Parameters*, 1994b).

The next development allowed a more detailed description of the gas/surface interaction. Following Schaaf and Chambre's suggestion (1961), three accommodation coefficients were developed that describe the degree of accommodation of the normal momentum, tangential momentum, and kinetic energy incident to the surface. Accommodation coefficients are statistical averages over the distribution function of the re-emitted molecules and over the distribution function of the incoming molecules. Because they are averages, detailed

information about the distribution functions is removed, so knowing the accommodation coefficients does not uniquely define the re-emitted distribution function. Accommodation coefficients are functions of the energy of the incoming molecule, incoming molecule/surface pair, and the material, surface temperature, and condition of the surface. Also, recent studies have shown that the values depend on the angles of the incident and reflected molecular streams. This discovery has led to the development of partial accommodation coefficients, which have not normally been incorporated into engineering design procedures (Collins and Knox, *Parameters,* 1994).

The accommodation coefficients are defined by a ratio of momentum flux differences. Components both normal and tangential to the surface must be taken into account separately. The following equations were first suggested by Schaaf and Chambre (1961), and have since become widely accepted:

$$\sigma' = \frac{P_i - P_r}{P_i - P_w} \qquad [3]$$

$$\sigma = \frac{\tau_i - \tau_r}{\tau_i} \qquad [4]$$

where σ' is the normal accommodation coefficient, σ is the tangential accommodation coefficient, P is the normal momentum flux and τ is the tangential momentum flux. The subscripts denote whether the flux is incident or re-emitted, and the w subscript refers to the component produced by a diffuse re-emission at the temperature of the surface, i.e. when the molecule comes to thermal equilibrium with the surface before being re-emitted.

Maxwell's two types of molecule reflection, specular and diffuse, are incorporated into the limits of the momentum accommodation coefficient coefficients. These models have generally been assumed to bracket the extremes of the aerodynamic coefficients. However, further studies have shown that this may not be the case after all (Collins and Knox, 1995). In the specular model, the normal momentum of the incoming flow is reversed, but the tangential momentum remains unchanged, so $\sigma' = \sigma = 0$. The diffuse case assumes that the re-emitted flux has completely accommodated to the wall temperature and follows a Maxwelllian distribution; therefore, $\sigma' = \sigma = 1$ (Demerest, 1996).

When the accommodation coefficients are substituted into the governing equations for free-molecule flow, the resulting equations are

$$C_P = \frac{1}{S^2}\left\{\begin{array}{l}\left(\frac{2-\sigma'}{\sqrt{\pi}} S\sin\delta + \frac{\sigma'}{2}\sqrt{\frac{T_w}{T_\infty}}\right) e^{-(S\sin\delta)^2} + \\ \left[\begin{array}{l}(2-\sigma')\left(S^2\sin^2\delta + \frac{1}{2}\right) + \\ \left(\frac{\sigma'}{2}\sqrt{\pi\frac{T_w}{T_\infty}} S\sin\delta\right)\end{array}\right]\left(1+erf(S\sin\delta)\right)\end{array}\right\} \qquad [5]$$

$$C_f = \frac{(\cos\delta)\sigma}{\sqrt{\pi S}}\left\{e^{-(S\sin\delta)^2} + \sqrt{\pi} S\sin\delta\left[1+erf(S\sin\delta)\right]\right\} \qquad [6]$$

where C_P is the pressure coefficient, C_f is the shear coefficient, S is the speed ratio, and δ is the angle between the incoming velocity and the surface tangent (see Figure 1) (Schaaf and Chambre, 1961). Equations [5] and [6] are integrated over

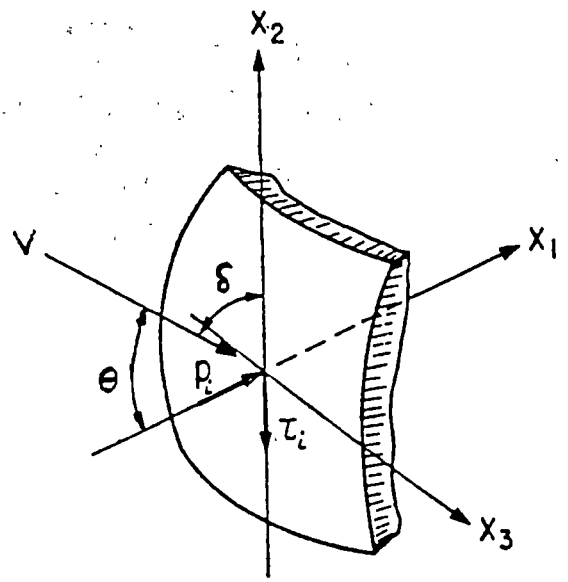

Figure 1. Coordinate System for Gas-Surface Interaction (Schaaf and Chambre, 1961)

the surface of the body exposed to the flow to determine the aerodynamic coefficients for lift (C_L) and drag (C_D).

One of the most useful methods of determining the aerodynamics of a body in the transition and free-molecule regimes is the Monte Carlo computational technique. This technique requires knowledge of the velocity distribution function of the molecules that are re-emitted after colliding with the surface. Traditionally, this interaction has been accounted for by the introduction of accommodation coefficients, but they are averages over the velocity distribution function and do not provide the statistical information necessary for the Monte Carlo calculations.

Collins and Knox (*Parameters*, 1994) suggested that a better option would be to use the Nocilla model instead of the accommodation coefficients. The Nocilla model gives an analytical form to the reflected distribution function, which is what is necessary for the Monte Carlo technique.

2.2 Previous Work

Satellite aerodynamics were first modeled in the 1960s. At that time, there was already a great deal of knowledge about the thermal accommodation coefficient, but not much was known about the momentum accommodation coefficients. In 1958, Schaaf and Chambre first introduced the now-accepted definitions for the momentum coefficients (Moore and Sowter, 1989). Since then, numerous papers have been published supporting one model or another. In fact, a recent paper by Knox, Collins and Liver (1991) identified over 200 references for analytical or experimental work dealing with gas-surface interactions. However, no measurements of the accommodation coefficients for satellite surfaces in orbit have ever been made.

Recently, Lyons and Hurlbut (1993) proposed an experiment to measure the lift produced by the Magellan spacecraft during the aerobraking maneuvers necessary to place Magellan in orbit around the planet Venus. Aerobraking is a method used to lower the satellite's orbit that involves using aerodynamic forces to slow the spacecraft. The proposed experiment would measure the aerodynamic forces produced on the two symmetric, flat solar panels at equal angles of attack in

what they called the "windmill" configuration. From these measurements, the lift and drag present on the spacecraft could be determined. This experiment would have been vital to the study of gas/surface interaction as it would have been the first direct measurement of momentum accommodation coefficients on well-defined geometry in orbit. Unfortunately, the proposed experiment never occurred, as there were no funds available. However, some data was collected during the aerobraking maneuvers that demonstrated the feasibility of the experiment.

Results of Studies by Collins

Although a great deal of research has been done in the area of gas-surface interaction measurements, there has generally been no attempt to correlate all the work and evaluate it. However, a recent study by Knox, Collins and Liver (1991) attempted to accomplish just that. They examined 17 curve-fit models and five empirical constants models to the applicable measurements (those which applied to orbital conditions) in an effort to take the very scattered work and apply it to real-life examples, namely a sphere, sphere-cone, wedge, and the NASA Aeroassist Flight Experiment (AFE). They found that all of the models basically agree on the value of atmospheric drag present on a body, but the atmospheric lift predictions varied greatly from the traditional diffuse model.

Out of this study, Knox, Collins and Liver (1991) recommended a curve-fit model, hereafter referred to as Model 17, as being a very promising model. This model allows for varying accommodation coefficients that depend on the incident

angle. The accommodation coefficients are defined as follows:

$$\sigma' = 1 - e^{-2.1(\cos\theta)^{1.6}}, \qquad [7]$$

$$\sigma = 0.6 - 0.4\left(\frac{45-\theta}{45}\right)^{1.6687} \quad \text{if } \theta \le 45°, \qquad [8.1]$$

$$\sigma = 0.6 \quad \text{if } \theta > 45°, \qquad [8.2]$$

where θ is the angle between the incoming flow and the vector normal to the surface (see Figure 1). Another model believed to have merit will be referred to as Model 15. For that model, the accommodation coefficients are defined as follows:

$$\sigma' = 1 - 0.9e^{-2.8(\cos\theta)^2}, \qquad [9]$$

$$\sigma = 0.9 - 1.2e^{-1.47(\sin\theta)^{0.75}} \quad \text{if } \theta > 8°, \qquad [10.1]$$

$$\sigma = 0.9 - 1.2e^{-1.47(\sin 8°)^{0.75}} \quad \text{if } \theta \le 8°, \qquad [10.2]$$

where θ is defined as before. This model yields results very similar to Model 17. It must be remembered that these models are the results of curve fits to the limited experimental data that is currently available and not assumed to be accurate without orbital measurements. Figure 2 shows measured data for the accommodation coefficients under orbital conditions. As can be seen, the data is widely scattered, which accounts for the fact that there are so many possible curve fits. Figure 3 shows how the normal and tangential accommodation coefficients for Models 15 and 17 vary with the incident angle. From the figures, the normal accommodation coefficient does a fair job of modeling the data, but the tangential accommodation coefficient is much more uncertain.

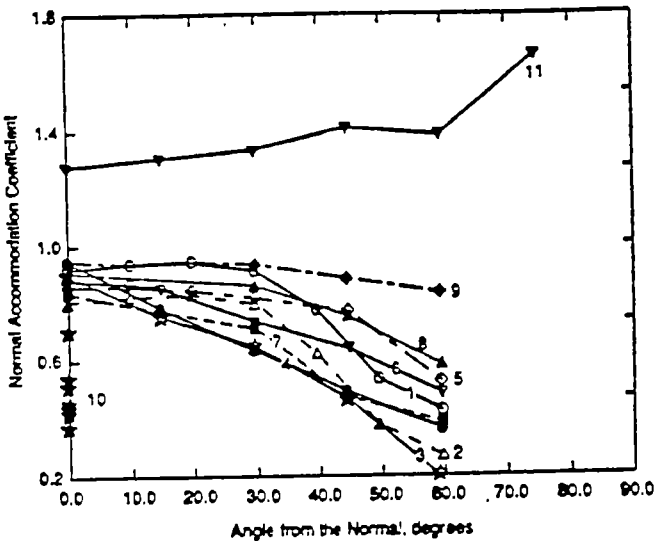

(a)

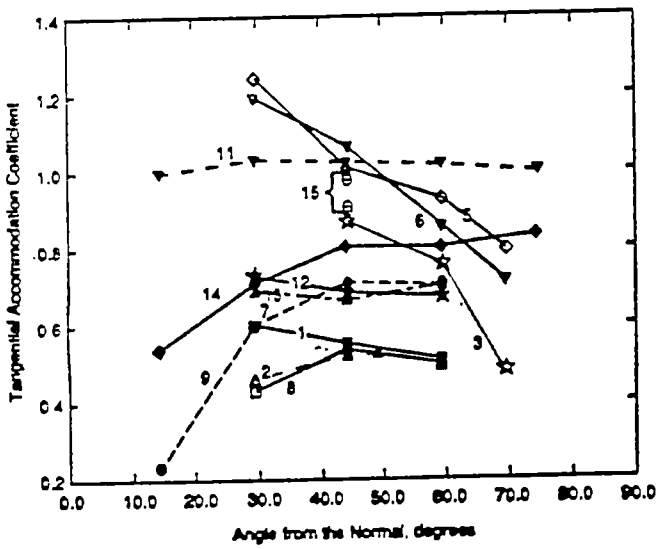

(b)

Figure 2. Momentum Accommodation Coefficient Measurements. (a) Normal Accommodation Coefficient, and (b) Tangential Accommodation Coefficient. (Collins and Knox, *Parameters*, 1994)

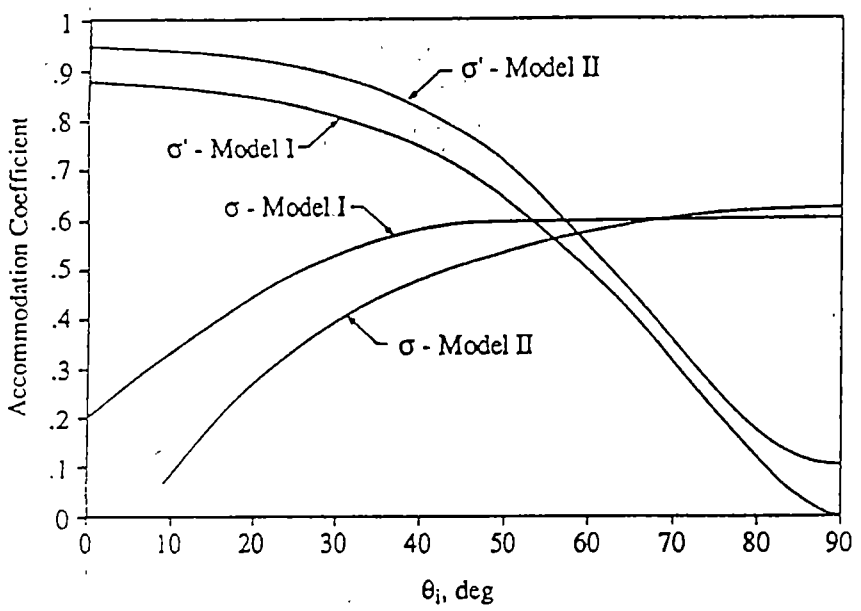

Figure 3. Momentum Accommodation Coefficients Given by Models 15 and 17 (Collins and Knox , *Determination of Wall,* 1994).

Results of Study by Demerest

The first European Remote Sensing Satellite (ERS-1), shown in Figure 4, was launched in 1989 for the purpose of increasing the understanding of interaction between the Earth's atmosphere and the oceans. The satellite was placed in a sun-synchronous polar orbit at about a 780 km altitude. Due to the nature of the orbit, the solar array only had to rotate about one axis (normal to the orbital plane) to maintain alignment with the sun. The main body of the 2.3 ton satellite was basically a box with a 2 m x 2 m base and 3 m high. A deployable solar array on one side of the satellite measured 12 m x 2.4 m, and was capable of rotating 360°

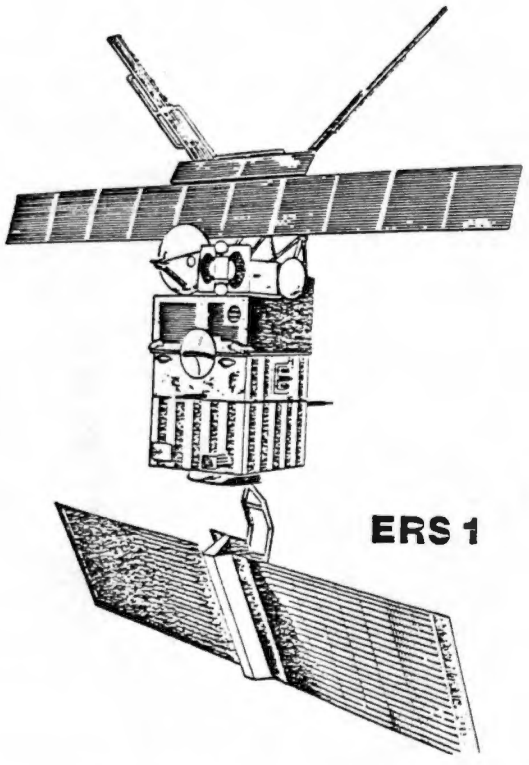

Figure 4. The European Remote Sensing Satellite (ERS-1) (Holdaway 1986).

during one orbit. The largest antenna on the other side of the main body measures 10 m x 1 m and is fixed to the satellite. (Francis et al., 1991)

As part of his master's thesis, Peter Demerest (1996) calculated the lift and drag present on the ERS-1 Satellite with the Supersonic/Hypersonic Arbitrary Body Program (S/HABP). To accomplish this, he compared the results of calculations using the diffuse model and calculations using Collins' Model 17. The ERS-1 was modeled simply as a 2 m x 2 m x 3 m box with a flat plate on each side, measuring 12 m x 2.4 m and 10 m x 1 m. He created several models that showed the solar array in different positions as the satellite orbited the Earth. Figure 5 is an example of the geometric model used.

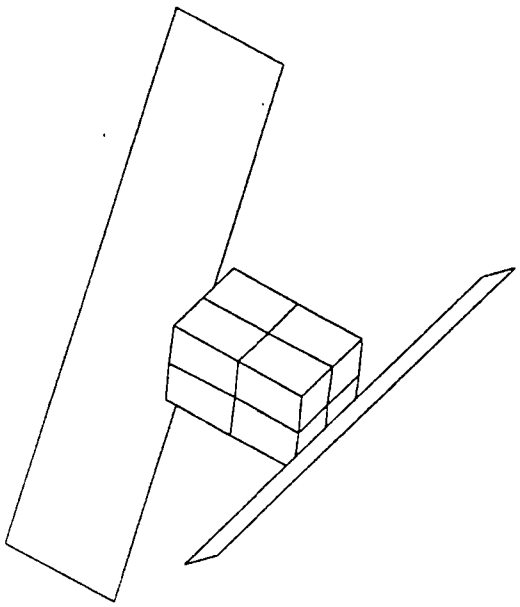

Figure 5. Geometric Model of the ERS-1 Satellite.

Demerest's calculations showed that while drag on the satellite remained basically the same for the two accommodation coefficient models, there was a substantial difference in the lift present on the satellite in orbit. The results of these calculations are shown in Figure 6. The calculated coefficients of lift and drag were then used in a computer program designed to calculate satellite orbits. The resulting orbital prediction was an improvement from the prediction using the aerodynamic coefficients based on the diffuse accommodation coefficients. However, there were still substantial differences between the measured and predicted orbits.

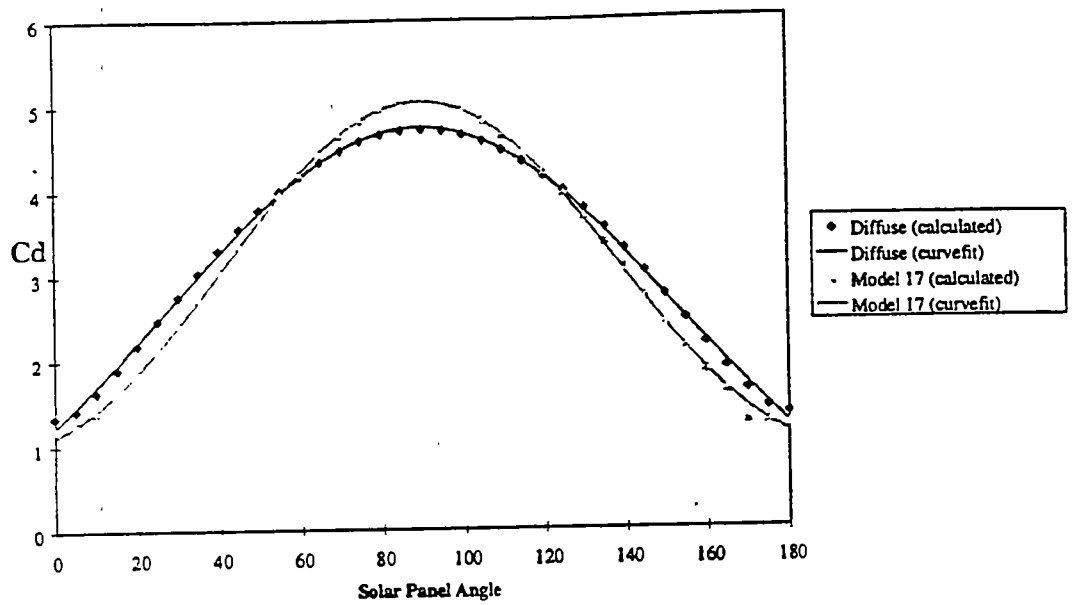

(a)

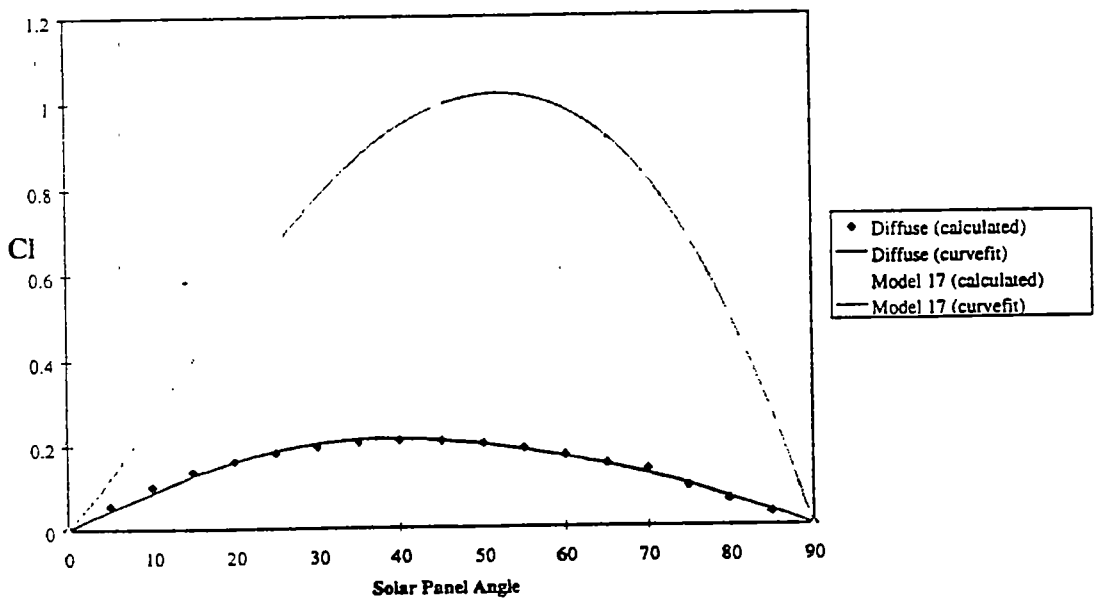

(b)

Figure 6. Aerodynamic Coefficients for the ERS-1 Satellite, (a) Coefficient of Drag, and (b) Coefficient of Lift (Demerest, 1996).

2.3 Viscous Effects on Complex Configurations Computer Code

The Viscous Effects on Complex Configurations (VECC) computer code is an updated version of the Supersonic/Hypersonic Arbitrary Body Program (S/HABP) developed for NASA by McDonnell Douglas Aerospace. The program takes an entered geometry and, for a given set of parameters, calculates the aerodynamic properties of the body. The original core of the S/HABP code was kept in tact, but it was surrounded with a graphical interface to make the program easier to use.

The VECC program is a combination of techniques and capabilities necessary in performing a complete aerodynamic analysis of supersonic and hypersonic shapes. "Although the program primarily uses local-slope pressure calculation methods that are most accurate at hypersonic speeds, its capabilities have been extended down into the supersonic speed range by the use of embedded flow field concepts." The purpose of the VECC program is as an engineering tool, not a research tool. Therefore, the accuracy of results for shapes and conditions where they are designed for may not be as good as other methods. However, for problems outside the range of linear or more exact methods, the results are very useful (Gentry et al. 1973).

The basic geometric unit used by the program is the surface element or quadrilateral method. This method allows any body to be represented as a set of points in space. A set of four points connected by straight lines becomes a quadrilateral surface element. To calculate forces, the surface element must be

converted to a plane element by calculating the vector normal to the surface, located at the center of the quadrilateral.

The aerodynamic characteristics of a body are calculated by finding the pressure and shear stress at the centroid of each surface element. The user may choose the method of force calculation. Several options (modified Newtonian, shock expansion, etc) are available, but this study is only concerned with the free-molecule flow method. The stresses calculated at the centroid are assumed to be the stresses over the entire surface. After the surface stresses are known, they are integrated over the entire body to give the aerodynamic forces and moments. (Demerest, 1996)

The free-molecule flow method calculates pressure and shear stress on a body for given Mach Number, geometry, angle of attack, and atmospheric conditions. The accommodation coefficients are assumed to be constant in the original VECC code, and are used directly in Equations [5] and [6]. An explanation of how to use the VECC program is given in Appendices A and B.

2.4 The Space Shuttle Orbiter

Since the late 1970s, the Space Shuttle has been America's transportation into space. The Shuttle fleet was designed to orbit earth at altitudes of 185 – 402 kilometers, and can carry payloads 60 feet long and 15 feet in diameter to space. The Orbiter carries a normal flight crew of eight, but can carry up to 10 in an emergency. The basic mission lasts for seven days. The Space Shuttle Orbiter is

121 feet long. 57 feet tall, and has a wingspan of 78 feet. The baseline center of gravity (cg) is as follows: X_{cg} = 1096 inches, Y_{cg} = 0.38 inches, and Z_{cg} = 377 inches (DeLombard, 1996). Obviously, these values vary slightly for each mission. The center of gravity information for all Shuttle missions is available on the World Wide Web at Johnson Space Center's website. Figure 7 shows a picture of the geometric model used in the analysis.

For this study, we were concerned with ten Space Shuttle flights: STS-6, 7, 8, 9, 11 (41B), 13 (41C), 24 (51B), 26(51F), 30 (61A), and 32 (61C). These particular missions were examined because the aerodynamic lift-to-drag measurements are readily available. Table 1 shows the designed centers of gravity for the ten missions during reentry. A complete listing of center of gravity locations for all missions is found in Appendix C.

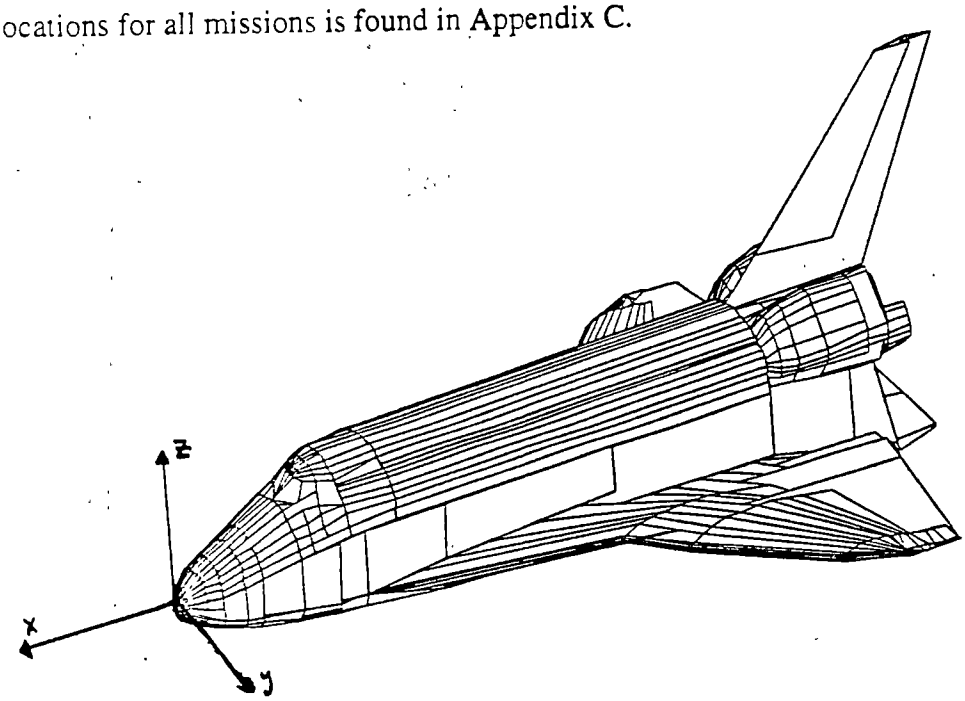

Figure 7. Geometric Model of the Space Shuttle Orbiter.

Table 1. Space Shuttle Orbiter Centers of Gravity (cite website)

Flight Number	Center of Gravity (inches from origin) X_{cg}	Y_{cg}	Z_{cg}	Launch Date
STS-6	-1101.2	0.4	368	4/4/83
STS-7	-1091.2	-0.6	370.1	6/18/83
STS-8	-1091.9	-0.1	370.4	8/30/83
STS-9	-1087.1	-0.1	370.7	11/28/83
STS-11 (41B)	specific values	not available		2/3/84
STS-13 (41C)	-1101.6	-0.1	368.2	4/6/84
STS-24 (51B)	-1085.4	-0.3	370.3	4/29/85
STS-26 (51F)	-1081.3	-0.6	370	7/29/85
STS-30 (61A)	-1085.2	-0.4	371.1	10/30/85
STS-32 (61C)	-1085.1	0.4	368.3	1/12/86

CHAPTER 3: CALCULATIONS

3.1 Lift-to-drag Ratio

Calculating the force coefficients for the Space Shuttle not only requires measuring the accelerations present on the Shuttle, but also requires knowledge of the freestream atmospheric conditions. However, the current experimental data that exists does not include any atmospheric measurements. Therefore, the lift-to-drag ratio, or L/D, is used as the aerodynamic parameter because the local dynamic pressure in each term cancels. The lift-to-drag ratio can be determined directly by the equation

$$\frac{L}{D} = \frac{R_a - \tan\alpha}{1 + R_a \tan\alpha}, \qquad [11]$$

where α is the angle of attack obtained from the onboard navigation gyro data, and R_a is the ratio of measured accelerations. The L/D measurement is of particular interest because it is sensitive to the gas/surface interaction, and therefore can reflect the differences in accommodation coefficients.

On the Space Shuttle, these accelerations were measured by the High Resolution Accelerometer Package (HiRAP) experiment, which measured accelerations down to 1.0 μg along the Orbiter's principal axes during reentry. The HiRAP experiment provides a time history of aerodynamic accelerations, from which the lift-to-drag ratio was calculated by averaging the data over a 1.0 second interval (roughly 175 data points) (Blanchard and Rutherford, 1984). At the start of re-entry, the Orbiter travels at an average speed of 7km/s. During a 1.0 second

interval, the atmospheric properties change very rapidly, which results in a change in the Knudsen Number. For example, as the altitude goes from 170 km to 163 km, the mean free path changes from 82 meters to 61 meters (*U.S. Standard Atmosphere*, 1976), resulting in the Knudsen Number changing from 2.05 to 0.656. The lift-to-drag ratio is a function of the Knudsen Number, so the change must be taken into account in some way. Obviously, averaging 175 data points taken in such varying conditions adds another uncertainty to the analysis.

The Orbital Acceleration Research Experiment (OARE) was the next generation of L/D measurement experiments to be flown on the Space Shuttle. The purpose of the experiment was to corroborate the HiRAP results and provide more precise measurements of L/D at high altitudes. The first OARE flight was in 1991 on STS-40, but no L/D measurements were made. Instead, it was determined that the device was working correctly, and two of the primary atmospheric models were evaluated (Blanchard et al. 1992). The OARE also flew on Space Shuttle mission STS-50. While acceleration measurements were made, no L/D information was available. This flight again served as a calibration flight, during which it was determined that there were some unknown causes of disturbance in the Shuttle environment that needed further exploration (Blanchard et al., 1993).

3.2 Experimental Measurements

Dr. Robert Blanchard, from the NASA Langley Research Center, has published a number of papers showing the experimental lift and drag measurements

from several Space Shuttle missions. For all the flights, he assumed a constant speed ratio and temperature ratio. The angle of attack was also assumed to be constant at 40°, since the Orbiter is required to reenter the atmosphere at that angle in order to complete a safe landing. Measurements of the angle of attack show that it was $40° \pm 2°$ for all flights, but the specific value for any data point was not given.

Dr. Blanchard's initial analysis of the first six flights (6, 7, 8, 9, 11, and 13) produced an average L/D value of 0.13 at an altitude of 160 kilometers, which was much higher than anyone had expected, especially since the diffuse scattering model predicted $L/D \cong 0.035$. Scatter in the data between flights was attributed to atmospheric conditions and the fact that the Orbiter altitude was near the threshold of the sensors (Blanchard, 1986). It must be noted, however, that atmospheric conditions were supposedly accounted for already in the fact that the L/D ratio was measured directly from accelerations. Further analysis on all ten flights resulted in a mean free-molecule flow L/D value of 0.056 at 160 kilometers altitude. This value assumes the Orbiter is in free-molecule flow, which is not the case, as will be explained in Section 3.4. This value is still greater than the traditional diffuse model value, but much lower than the previous estimate. Blanchard and his associates attributed the significant reduction in the lift-to-drag ratio in part to corrections for the auxiliary power unit (APU) and other biases from earth calibrations in a 1 g environment. Figure 8 shows the measured values of the L/D parameter for a number of flights. The data points in column (a) are from the first

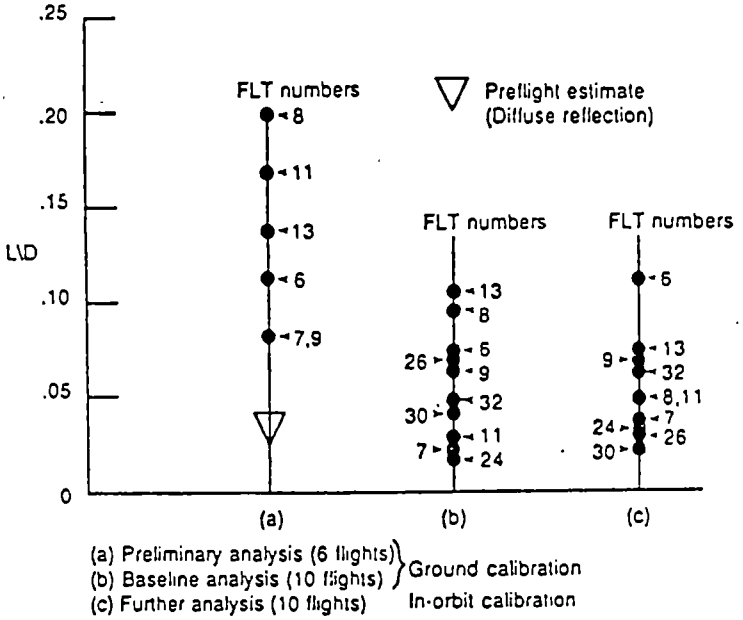

Figure 8. Measured Lift-to-drag Ratio for the Space Shuttle Orbiter (Blanchard and Larman 1987).

six flights, column (b) shows the results of all ten flights with ground calibrations accounted for, and column (c) shows the results for the same ten flights after in-orbit biases are removed.

3.3 Input Parameters/Conditions

For this study, the same Orbiter conditions documented in Dr. Blanchard's papers were used to make the assumptions as realistic as possible. Therefore, we used a constant speed ratio of 9.03, temperature ratio of 0.25, and an altitude of 160 km (524,934 feet). At this altitude, the Space Shuttle is in reentry, and the angle of attack is 40°. Basic Orbiter dimensions were used, but the exact center of gravity

location for each mission, except STS-11 (41B), was used. Since the information for STS-11 (41B) was unavailable, the baseline locations were used.

The method used to calculate the aerodynamic coefficients was simple. The two variable accommodation coefficient models mentioned in this thesis were added to the existing computer code, as described in Appendix A.1 (the diffuse model was already in the code). Then, for each mission, the lift and drag coefficients were calculated using each of the three different models. This process resulted in three different sets of aerodynamic coefficients for each Orbiter flight, allowing the author to compare the effect of the accommodation coefficient models on the calculations.

3.4 Assumptions

Free-molecule Flow

In the Earth's atmosphere, for the Shuttle to be in free-molecule flow, and assuming a characteristic length of 40 meters, the altitude would have to be about 250 km. At 160 km, which is the altitude used in this thesis and also where Dr. Blanchard made his highest elevation measurements, the Knudsen number is closer to one. Therefore, the Shuttle at a 160 km altitude during reentry is in a transition flow regime, which is the region where neither continuum flow nor free-molecule flow alone defines the fluid behavior. Blanchard assumes free-molecule flow to occur at 200 km, but this is still in the transition regime. Regardless of this fact, the assumption was made that the free-molecule equations applied.

Constant Value for Specific Heat Ratio

No mention was made in any of the documentation about the specific heat ratio, γ, most likely because it is not necessary in the measurements. However, the computer program requires a value for Mach Number, so 1.4 was used as the assumed value of the specific heat ratio. This is not accurate as the standard atmosphere shows there to be almost equal parts of nitrogen, N_2, and atomic oxygen, O, in the atmosphere at 160 km.

Constant Temperature Ratio

Since the atmospheric temperature was not recorded for each Shuttle mission, the value must be assumed from traditional atmospheric models. We know, however, that the temperature of the atmosphere changes over time, so assuming a constant atmospheric temperature for a number of Orbiter flights is questionable. Even though the temperature may change, the temperature ratio is thought to only vary between the values of 0.20 to 0.50, which are considered to be the limiting values that the Orbiter could encounter (Blanchard, 1986).

Constant Speed Ratio

Blanchard's results assume a constant speed ratio of 9.03. For this to be true, the speed of the Orbiter must be around 6600 m/s (assuming standard atmospheric properties, see Appendix D). From comparisons with published

values of orbital speed versus altitude (see Figure 9), at altitudes of over 100 km, the speed of the Orbiter is more on the order of 7400 m/s. If the speed of 7400 m/s is used, the resulting speed ratio is 10.5, which seems more reasonable.

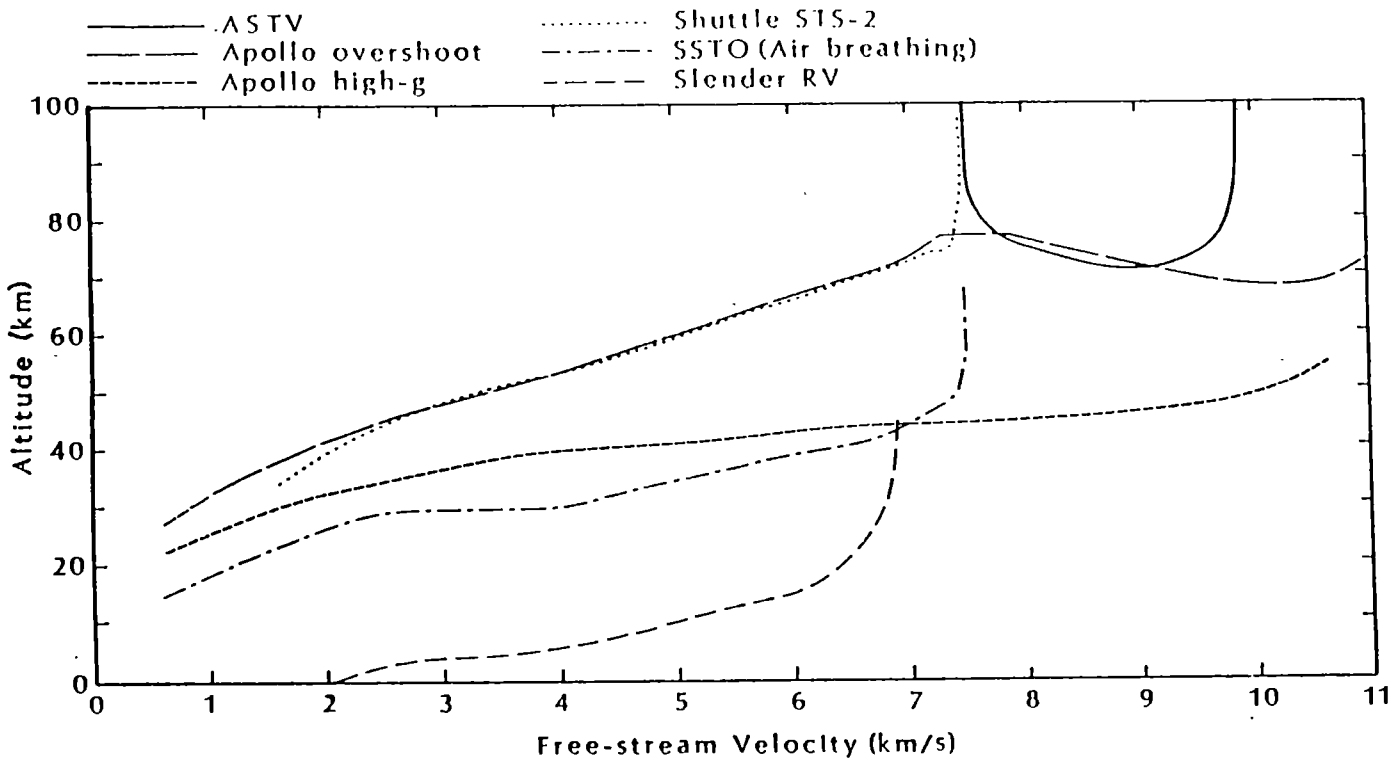

Figure 9. Velocity/Altitude Parameters for Several Re-entry Vehicles (Bertin, 1994).

CHAPTER 4: RESULTS

4.1 Results of Calculations

It was found that the minor changes in the center of gravity for each mission did not measurably affect the results. For each mission, the center of gravity was kept within such tight margins that the change from the baseline value was not a factor in the calculations. Therefore, the resulting aerodynamic coefficients for each mission were not listed, but the value was simply noted once for each model.

In the comparison of results, the measured L/D is the result of averaging the re-entry values from the ten flights. The preliminary data point is the L/D value of 0.13 that Blanchard published after analyzing the first six flights. The corrected L/D value of 0.056 is an average for all ten flights with biases taken into account. No measured values for the coefficients of lift and drag were given with the data, only the lift-to-drag ratio. Table 2 shows the results of the calculations.

The current calculations, as well as previous work (Knox, Collins and Liver, 1991), show that the drag calculated by all three accommodation coefficient models is comparable. Both Models 15 and 17 predict a lift value that is one order of magnitude greater than the diffuse model suggests. If we assume that the drag calculated by the diffuse model is correct, we can calculate a lift-to-drag ratio normalized by the diffuse drag coefficient. When the lift-to-drag ratio is normalized by the diffuse drag, the difference between the Models 15 and 17 disappears. The normalized results are in Table 3.

Table 2. Calculated Aerodynamic Coefficients

Model	C_L	C_D	L/D
Measured Data	(10 flight	average)	0.13 (Preliminary)
			0.056 (Corrected)
Diffuse	0.41302	11.94725	0.03457
Model 15	3.84603	9.89306	0.38876
Model 17	3.85521	10.54914	0.36545

(Assuming S=9.03, γ=1.4, T_w/T_{inf} = 0.25)

Table 3. Normalized Calculated Aerodynamic Coefficients

Model	$L/D_{diffuse}$	L/D (calculated)
Measured (average	for 10 flights)	0.13 (preliminary)
		0.056 (corrected)
Diffuse	0.03457	0.03457
Model 15	0.3219	0.38876
Model 17	0.3227	0.36545

(Assuming S=9.03, γ=1.4, T_w/T_{inf} = 0.25)

From the Tables 2 and 3, it is clear that the measured lift-to-drag ratio is lower than the values predicted by the variable accommodation coefficient models, but higher than the diffuse model's prediction, even when the biases are removed. Therefore, the diffuse model under-predicts the amount of lift present on the Shuttle Orbiter, as was suspected. However, it is also clear that the variable accommodation coefficient models vastly over-predict the amount of lift present. Figure 10 shows how the present calculated result compares with the measured lift-to-drag ratios.

4.2 Sensitivity Tests

Many assumptions of atmospheric conditions were made in the previous work, in measurements, and in this thesis. In order to test the validity of these assumptions, sensitivity tests were performed to see how varying certain parameters affected the aerodynamic properties. Also, the effect of environmental conditions on the accommodation coefficient models was of interest.

Temperature Ratio

To test how sensitive the aerodynamic properties were to varying temperature ratios, the lift-to-drag ratio for one mission was calculated with temperature ratios ranging from 0.20 to 0.50 (where 0.25 is the value from the experiments). As can be seen from the Table 4, the temperature ratio has an effect

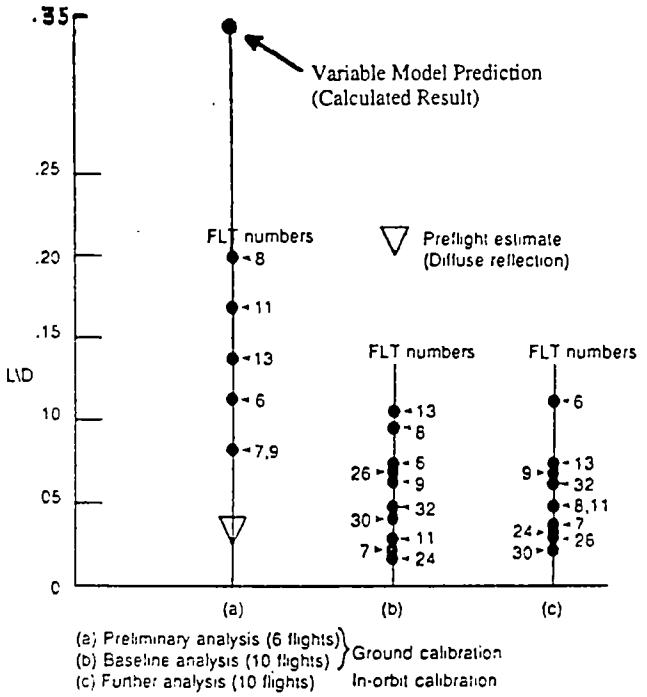

Figure 10. Comparison of Calculated and Measured Lift-to-drag Ratios.

Table 4. Effects of Varying Temperature Ratio

T_w/T_{inf}	L/D Diffuse	L/D Model 15	L/D Model 17	L/D Measured
0.20	0.03155	0.38698	0.36390	
0.25	0.03457	0.38876	0.36545	0.13 / 0.056
0.30	0.03728	0.39036	0.36685	
0.40	0.04207	0.39319	0.36933	
0.50	0.04624	0.39565	0.37149	

(Assuming S=9.03, γ=1.4)

on the lift-to-drag ratio. Moreover, notice that the temperature ratio has a much greater influence on the diffuse calculations than on those using the variable accommodation coefficient correlations. Thus, knowledge of the temperature ratio is much more important for diffuse scattering than for lobular scattering, and should have been reported in each paper published on the subject.

Speed Ratio

Since there is a great deal of uncertainty in the published speed ratio value, the calculations were done using two different speed ratios in an attempt to determine the effect it had on the lift-to-drag ratio. The first speed ratio was Blanchard's published value of 9.03; the second speed ratio was the more realistic 10.5. Assuming a specific heat ratio of 1.4, the resulting Mach Numbers were 10.79 and 12.55, respectively. From Table 5, we can see the change in speed ratio makes a small impact on the lift-to-drag ratio for the diffuse model. Models 15 and 17 are not affected by the varying speed ratio. Again, it is much more important to know the actual speed ratio for diffuse scattering than for lobular scattering.

Angle of Attack

Another assumption Blanchard made in his measurements was a constant angle of attack for the Orbiter during reentry. He states that the angle of attack only varies by ±2°, and therefore does not affect the results. In an attempt to verify

Table 5. Effects of Varying Speed Ratio

Speed Ratio	L/D Diffuse	L/D Model 15	L/D Model 17
9.03	0.03457	0.38876	0.36545
10.5	0.02952	0.38757	0.36417

(Assuming γ=1.4, T_w/T_{inf} = 0.25)

this assumption, calculations were done with the angle of attack varying from 38° to 42°. As Table 6 shows, the angle of attack does have an effect on the aerodynamic coefficients, although it is minor. The coefficient of drag was more affected by the change in angle of attack than the coefficient of lift, but all three models were affected equally. So, the angle of attack is an important factor in calculating the aerodynamic forces present on a body regardless of what accommodation coefficient model is used, but a two-degree change makes little difference.

Other Factors

There are a variety of other factors that may affect vehicles in low-earth orbit that cannot be examined in this study. One such factor is the solar cycle activity. Solar radiation has been known to exert a force on satellites of equal

Table 6. Effects of Varying Angle of Attack

Angle of Attack	L/D Diffuse	L/D Model 15	L/D Model 17	L/D Measured
38°	0.03544	0.39429	0.37598	
40°	0.03457	0.38876	0.36545	0.13/0.056
42°	0.03361	0.38232	0.35382	

(Assuming S=9.03, γ=1.4, T_w/T_{inf} = 0.25)

magnitude to the aerodynamic forces of lift and drag. Also, the solar activity changes the composition and temperature of the atmosphere at a given altitude. Both are factors in the speed ratio. Since no data on the solar cycle activity was noted during the experiments, there is no way we can draw any conclusions about how it may have affected the measured forces on the Space Shuttle Orbiter. Figure 11 shows the solar cycle activity for each year with the dates of the ten Shuttle missions noted. As can be seen, the missions under consideration are all within a four-year period during which time the solar cycle activity was decreasing. During the four years, the number of sunspots decreased from about 70 per year to about 10 per year.

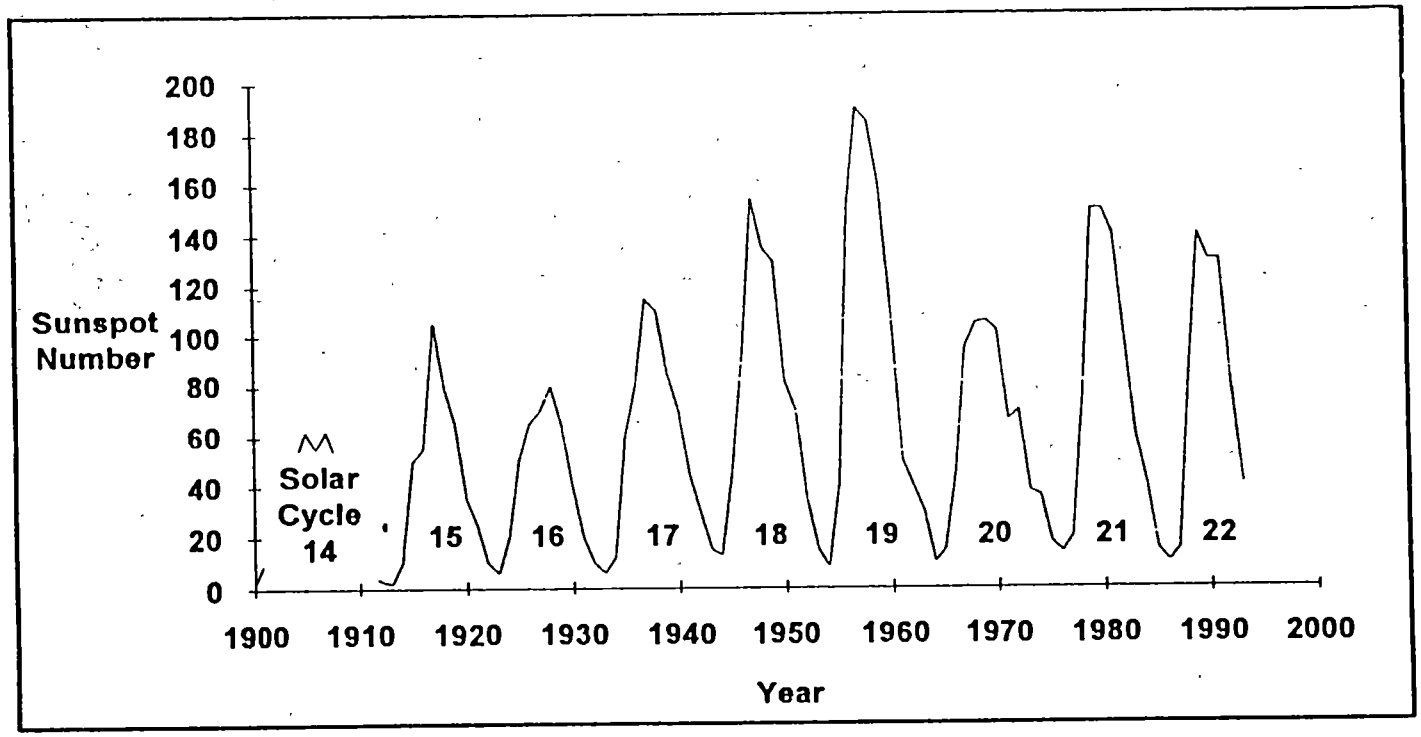

Figure 11. Solar cycle Activity (Tribble, 1995).

CHAPTER 5: CONCLUSIONS

Although there has been a great deal of research done to model the free-molecule flow regime, there is still much work that needs to be done to increase understanding of the low-earth orbit atmosphere. Orbital conditions are difficult, if not impossible, to recreate in the laboratory, so scientists have to rely on theoretical, statistical models. Previous studies on satellites have shown that new, variable accommodation coefficient models can produce more accurate values for the aerodynamic coefficients than the traditional diffuse model, but the data is full of uncertainties. This data, however, was obtained for smooth surfaces, while the Shuttle Orbiter tiles are very rough and irregular.

The goal of this thesis was to integrate variable accommodation coefficient models into the VECC computer code used to calculate the aerodynamic forces present on a body, and then to compare the aerodynamic predictions using high energy accommodation coefficient measurements with the measured values for the Space Shuttle Orbiter. Measurements of the Orbiter's lift-to-drag ratio during reentry were at least twice as great as those predicted by the diffuse model, signifying that there is more lift present than traditionally thought, and that the molecules scatter from the Orbiter's tiles in a non-diffuse manner. However, calculations using the variable accommodation coefficient models predicted a lift-to-drag ratio that was one order of magnitude greater than either the prediction from the diffuse model or the actual measured values. From this analysis, it is

obvious that the variable accommodation coefficient models do not apply to the Space Shuttle Orbiter. The curve fits were developed from data for smooth engineering surfaces, and the rough ceramic tile surface of the Shuttle Orbiter obviously reflects the molecules in a more diffuse manner. Even though a previous study by Peter Demerest (1996) used the variable accommodation coefficient model to improve the orbital prediction for a satellite in orbit, the use of the same model in this thesis did not improve the prediction for the Shuttle Orbiter. Therefore, it must be concluded that the variable accommodation coefficient models do not apply to rough surfaces, but would most likely apply to the Space Station, its solar panels, and other smooth surfaces.

Finally, it was noted that the L/D predictions for the Shuttle Orbiter using the diffuse scattering model were very sensitive to wall temperature, atmospheric temperature, and the atmospheric composition. It is very important to measure these parameters if there is ever any hope of comparing measurements and predictions. From this, it must be concluded that atmospheric information and the wall surface temperature are necessary, even for lift-to-drag ratio measurements.

CHAPTER SIX: RECOMMENDATIONS

As previously stated, we still do not have a good understanding of aerodynamics in the space environment, including free-molecule flow and especially the transition regime. With improved understanding come better designs for future spacecraft as well as better simulators here on earth. If single-stage-to-orbit vehicles and precise orbit determination are ever to become reality, a great deal of research needs to be done.

The biggest problem with the use of accommodation coefficient models for calculating aerodynamic forces on a surface is the lack of actual measurements taken in orbit. Experiments should be performed in orbit, coupled with direct measurements of atmospheric temperature, density, etc, in order to produce real data to use in comparing and improving the mathematical models. Scientists would no longer have to depend on data from non-engineering surfaces, inappropriate flow regimes, or accelerated ions here on Earth. Experiments such as the Magellan "windmill" experiment would give direct measurements of the momentum accommodation coefficients, which could then be used to correct and/or verify gas/surface interaction models.

While we were able to add the two new accommodation coefficient models to the VECC code, this is really only a temporary solution. A better option would be to use a Nocilla model rather than the accommodation coefficient models. However, regardless of whether an accommodation coefficient model or a Nocilla

model is used, there is still the task of integrating the equations into the code more efficiently. Currently, the user must be able to access the source code in order to change the chosen accommodation coefficient model. This is very cumbersome and time-consuming. If the different models are going to be used frequently (as in a comparison study like this one), the source code should be changed so that a specific model could be chosen from within the program. This could be easily accomplished by adding a simple if-then loop to the *force.f* program. In this way, all models would be accessible without having to constantly recompile the program. Instead, the box labeled *Free Molecular Flow* in the *Run Setup* subroutine could be used to select the model. A change of this nature would make using the code easier and more efficient.

Once construction is completed, an analysis similar to this thesis should be performed to see how the variable accommodation coefficients apply to the Space Station. It is most likely that the results would show the diffuse model under-predicting the amount of aerodynamic lift present, and the variable accommodation coefficient models would produce a much more accurate prediction of the free-molecule flow behavior and of the aerodynamic forces acting on the Space Station.

REFERENCES

REFERENCES

Bertin. J. J., *Hypersonic Aerothermodynamics,* American Institute of Aeronautics and Astronautics, Inc., Washington, D. C., 1994.

Blanchard, R. C., and Rutherford, J. F, "Shuttle Orbiter High Resolution Accelerometer Package Experiment: Preliminary Flight Results," 22nd Aerospace Science Meeting, AIAA Paper No. 84-0490, Reno, Nevada, January, 1984.

Blanchard, R. C., "Rarefied Flow Lift-to-drag Measurements of the Shuttle Orbiter," Proceedings of the 15th Congress of the International Council of the Aeronautical Sciences, ICAS 86-2.10.2, London, England, September, 1986.

Blanchard, R. C., and Larman, K. T., "Rarefied Aerodynamics and Upper Atmospheric Flight Results From the Orbiter High Resolution Accelerometer Package Experiment," AIAA Paper No. 87-2366 (1987).

Blanchard, R. C., Nicholson, J. Y., and Ritter, J. R., "Preliminary OARE Absolute Acceleration Measurements on STS-50," Joint "L+1" Science Review, Huntsville, Alabama, September, 1993.

Blanchard, R. C., Nicholson, J. Y., and Ritter, J. R., "STS-40 Orbital Acceleration Research Experiment Flight Results During a Typical Sleep Period," Microgravity Science and Technology, Vol. 2, 1992.

Collins, F. G., and E. C. Knox. "Determination of Wall Boundary Conditions for High-Speed-Ratio Direct Simulation Monte Carlo Calculations," Journal of Spacecraft and Rockets, Vol. 31, No. 6, 1994, pp. 965-970.

Collins, F. G., and Knox, E. C., " Parameters of Nocilla Gas/Surface Interaction Model from Measured Accommodation Coefficients," AIAA Journal, Vol. 32, No. 4, April 1994.

Collins, F. G., and Know, E. C., "Review of the Expected Magnitude of Aerodynamic Forces in Free-Molecule Flow," 33rd Aerospace Science Meeting, AIAA Paper No. 95-0756, Reno, Nevada, January, 1995.

Crowther, R., and Stark, J., "The Determination of the Gas-Surface Interaction From Satellite Orbit Analysis as Applied to ANS-1 (1975-70A)," Planetary Space Science, Vol. 39, No. 5, 1991, pp. 729-736.

DeLombard, R., "Compendium of Information for Interpreting the Microgravity Environment of the Orbiter Spacecraft," NASA Technical Memorandum 107032, August 1996.

Demerest, P., "Aerodynamic Effects on an Earth Orbiting Satellite," Masters Thesis, The University of Tennessee Space Institute, August 1996.

Francis, R., et al, "The ERS-1 Spacecraft and Its Payload," ESA Bulletin, No. 65, 1991, pp. 27-48.

Gentry, A. E., Smyth, D. N., and Oliver, W. R., " The Mark IV Supersonic-Hypersonic Arbitrary-Body Program," AFFDL-TR-73-159, Vol. 2, 1973.

Hansen, J. E., et al, "Global Climate Data and Models: A Reconciliation," Science, Vol. 281, 14 August 1998.

Holdaway, R., "Assessing Orbit Determination Requirements for ERS-1," 24th Aerospace Science Meeting, AIAA Paper No. 86-0403, Reno, Nevada, January, 1986.

Knox, E. C., Collins, F. G., and Liver, P. A., "Engineering Assessment of Gas/Surface Interactions in Free0Molecular Aerodynamics," 22nd Fluid Dynamics, Plasma Dynamics & Lasers Conference, AIAA Paper No. 91-1747, Honolulu, Hawaii, June, 1991.

Lyons, D. T., and Hurlbut, F. C., "Measuring Lift Coefficient in Free Molecular Flow While Aerobraking Magellan," Rarefied Gas Dynamics: Space Science and Engineering, Vol. 160, 1993.

Moore, P., and Sowter, A., "Application of a Satellite Aerodynamics Model Based on Normal and Tangential Momentum Accommodation Coefficients," Planetary Space Sciences, Vol. 39, No. 10, 1991, pp. 1405-1419.

Schaaf, S. A., and Chambre, P. L., *Flow of Rarefied Gases*, Princeton University Press. Princeton, New Jersey, 1961.

Tribble, A. C., *The Space Environment: Implications for Spacecraft Design*, Princeton University Press, Princeton, New Jersey, 1995.

U. S. Standard Atmosphere, 1976, U. S. Government Printing Office, Washigton, D.C., 1976.

APPENDICES

APPENDIX A

THE VISCOUS EFFECTS ON COMPLEX CONFIGURATIONS (VECC) COMPUTER CODE

A.1 Running Viscous Effects on Complex Configurations

The Viscous Effects on Complex Configurations computer code, used to calculate the aerodynamic coefficients for complex geometry, seems to work best on a Silicon Graphics platform. The program is made up of five subprograms that are compiled using the individual makefiles. There are several bugs that have to be fixed before the program will compile correctly, mostly minor details such as renaming blank common blocks and personalizing some settings for the specific computer being used. Once each subprogram has been compiled, the main makefile (found in the main directory) can be compiled. This makefile results in the executable file that runs the entire program. Once in the main program, everything is menu-driven.

The VECC code is capable of creating geometry, but the process is inefficient and time-consuming. However, a file created in a different program such as CAD or VUAERO can be imported into VECC with little or no difficulty. Once the basic geometry has been formed, VECC can be used to modify the object.

Certain changes were made in the main code to allow for various accommodation coefficient models. Changes were necessary in only one place in the code. The new coefficient models were added in the *Mk5* sub-directory, program *force.f*, line 420. At this time, there is no way to select which model is desired once in the program. Therefore, before starting the program, *force.f* must be modified to show the desired model. The three models used in this study have

already been added to the program, so selection of a particular model is simply accomplished by removing the comment notation from the chosen model, and commenting out the other models. The program must then be re-compiled, which is easily accomplished in the *Mk5* sub-directory by typing the command *make -f makefile5*. Once this step is completed, the program is started and run as usual. However, any time the user wishes to change the accommodation coefficient model used in the calculations, this process must be repeated. Note: The makefile will only recompile programs that have been modified since the last compilation, so the process only takes a few moments.

A.2 Using Viscous Effects on Complex Configurations

Performing calculations using the VECC code is relatively simple. Once the program is started, a geometry file can be opened. The latest version of the code (version 5) uses files ending with the extension *.mk5*, but can read files with the *.geo* extension. After the geometry file is opened, changes to the object can be made by selecting specific points, cross-sections, or panels. All geometry files are made up of a series of panels. For example, the Space Shuttle has several panels such as the wing, vertical tail, etc. Before any calculations can be done, the panels have to be grouped together to make components. Analysis is done on a particular component, so any panel that makes up part of the geometry to be analyzed must be included in the component.

Components are added by using the *Panel Grouping* option found in the *Edit* menu. The desired panels are highlighted by selecting them with the mouse and clicking the left mouse button. Multiple panels can be selected by holding down the shift key while selecting. Once all the panels are selected, the component is created by selecting *Add Component*. The default name for the component is *unnamed*, but that can be changed by clicking on the name and typing a new name. Once the component is added, the analysis can continue. After each step is completed, the user would be wise to save the file by selecting *Save/Save As* in the *File* menu. Regardless of whether the initial geometry file had the *mk5* extension or not, all files should be saved with that extension.

Several editing options are now available. The user must define the units to be used in the calculations. This is done by selecting the *Input Units* option in the *Edit* menu. Units choices include meters, centimeters, millimeters, feet, and inches. The location of a specific point can be followed through any geometry manipulation. The point is selected by clicking on the desired point with the middle mouse button (if available), or by pressing both mouse buttons together. The point identification number and x-y-z coordinates will appear in the bottom of the screen. Different viewing angles are also available in the *Display* menu.

The next step in the analysis is to create a specific run for the calculations. This process begins by selecting *Run Setup* in the *Edit* menu. The program then asks you to select which component you wish to analyze. The next option is whether viscous or inviscid analysis is desired. For this study, the inviscid flow option was chosen. At this point, a sub-menu appears that requests values for dynamic pressure ratio, temperature ratio (T_w/T_{inf}), and two boxes for defining the accommodation coefficients. These two boxes are labeled *Free-molecular Flow* and *0=Newtonian 1=Diffuse*. Due to additions made to the code, these boxes no longer define the accommodation coefficients. Therefore, they are left at 1.0, and the desired coefficient model is selected as described in the preceding section. The dynamic pressure ratio is left at the default of 1.0, and the desired value of temperature ratio is entered. Once all the values are entered, pressing the *OK*

button brings the user back to the main menu. Previously defined runs may be edited by highlighting and selecting *Edit* on the first submenu.

The next step in setting up the analysis is to define the case. To begin this step, select the *Case Setup* from the *Edit* menu. If a case has already been defined, it is possible to edit the previous case by highlighting the case name. Otherwise, a new case must be added. The program also asks what runs should be included in the case. Any specific existing run or all runs may be selected and added to the case setup. The physical properties of the body to be analyzed are found under the option *Edit Flight Conditions/Reference Quantities* in the *Case Setup* submenu. The first set of boxes allow for the geometric properties to be added, i.e., frontal area, length, span, and center of gravity locations. The next section asks for atmospheric conditions such as Mach number, altitude, and what type of atmosphere is present. Finally, different angles of attack may be selected for analysis. Once all the boxes have been filled, pressing the *OK* button brings the user back to the main menu.

Now that the run and case have been set up, it is time to perform the calculation. To start the calculations, *S/HABP Mk V* must be selected under the *Analysis* menu. For relatively simple geometry (including the Space Shuttle), analysis takes less than 30 seconds. The results can then be viewed independently of the VECC program. The output is saved in a file with the same name as the geometry file, followed by the *.out* extension.

APPENDIX B

VECC MAKEFILES

B.1 Main Program Makefile

```
all:
	cd Gui/Quad; make -f makefile5
	cd Gui;  make -f makefile5
	cd Plot; make -f makefile5
	cd Mk5;  make -f makefile5
	cd Trim; make -f makefile5

clean:
#	rm -f vecc
#	rm -f hplot
#	rm -f mk5
#	rm -f trim
	rm -f Gui/*.o
	rm -f Plot/*.o
	rm -f Mk5/*.o
	rm -f Trim/*.o
	rm -f Gui/Quad/*.o
```

B.2 Gui Makefile

```
FOR      = f77 -32
DEBUG    = -g
CFLAGS     =  -D_NO_PROTO -DSYSV
FFLAGS   =
LIBS     = -lXm -lXt -lX11 -lPW -lsun -lm
LIBS     = -lXm -lXt -lX11 -lPW -lm
INCLUDES = -I/usr/include/X11
LDFLAGS  =
XOBJS    =
OBJS =    main.o     widgets.o   buttons.o flowf.o    \
     menubar.o  menu.o     xmenu.o     busy.o
build.o    \
     help.o     fgl.o      xdraw.o     globals.o
habpio.o  \
     pscript.o  futil.o    3dbuild.o   fdraw.o
picking.o \
     inoutput.o stream.o   habp.o      dialog.o  case.o
trim.o

# special stuff for some SUN systems
#LIBS      = -lXm -lXt -lX11 -lm
#INCLUDES = -I/usr/openwin/include

# special stuff for Hewlett Packard
#INCLUDES = -I/usr/include/X11R5  -
I/usr/include/Motif1.2
#LDFLAGS  = -L/usr/lib/X11R5 -L/usr/lib/Motif1.2
#FOR      = fort77
#XOBJS    = hp_getarg.o
#LIBS       = -lXm -lXt -lX11 -lm


../test:  $(OBJS) $(XOBJS)
     rm -f $@
     $(FOR) -o $@ $(LDFLAGS) $(OBJS) Quad/*.o $(XOBJS)
$(LIBS)

.c.o:
     rm -f $@
     $(CC) -c $(CFLAGS) $(DEBUG) $(INCLUDES) $*.c
```

```
.f.o:
	rm -f $@
	$(FOR) -c $(DEBUG) $(FFLAGS) $*.f

lint:	$(OBJS) $(XOBJS)
	lint $(INCLUDES) *.c > lint.out
```

B.3 Mk5 Makefile

```
#
#  Makefile for S/HABP Mk 5
#

#
# set up logicals and flags for compile options
#

RM = rm -f
CC = cc
FOR = f77 -32

#CFLAGS    = -g
CFLAGS =
FFLAGS =  -C -check_bounds
DEFINES = -DSYSV
INCLUDES = -I/usr/include
LIBS =  -lX11 -lPW -lsun -lm
LIBS =  -lX11 -lPW -lm

#
# list files that comprise the S/HABP Mk 5 program
(Main Object files)
#

MOBJ =    acone.o \
     aero.o \
     aircft.o \
     arcos.o \
     arsin.o \
     atmos.o \
     auxili.o \
     bbstrt.o \
     bl.o \
     blcf.o \
     block.o \
     blunt.o \
     blunts.o \
     cada.o \
     calc.o \
     cfinpt.o \
```

```
cmpexp.o \
compr.o \
cone.o \
conea.o \
contrl.o \
cpinpt.o \
cubic.o \
cubspln.o \
curvft.o \
deriv.o \
dot_product.o \
egamma.o \
ellip.o \
elp1.o \
erf.o \
erff.o \
erfh.o \
errf.o \
eval.o \
expan.o \
expand.o \
ffbody.o \
ffinpt.o \
ffree.o \
ffsose.o \
ffspec.o \
ffsurf.o \
flntrp.o \
flow.o \
force.o \
formp.o \
forsf.o \
fprint.o \
fsubc.o \
funct.o \
fuse.o \
gencut.o \
geom.o \
getpdat.o \
gett.o \
gradnt.o \
header.o \
headr3.o \
```

```
heat.o \
idlgs.o \
iele.o \
int1.o \
int2.o \
integ.o \
interp.o \
isort.o \
lamnar.o \
least_sqr.o \
ledge.o \
lgrnge.o \
make_surf.o \
mark5.o \
merid.o \
mis2.o \
modnew.o \
monitr.o \
mout.o \
nacel.o \
ncone.o \
newtpm.o \
normal.o \
nrml.o \
obli01.o \
oblidl.o \
obliqe.o \
oblrgs.o \
obltbl.o \
order.o \
outd.o \
plate.o \
plunge.o \
poly.o \
precal.o \
pres.o \
presot.o \
profil.o \
prop.o \
punch.o \
qc.o \
rcstr.o \
rdydx.o \
```

```
rgs.o \
rgsair.o \
rgsdr.o \
rgsfp.o \
rgsfr.o \
rgsi.o \
rgsp.o \
rgspl.o \
rgsrl.o \
rgsser.o \
rnewtn.o \
romu.o \
root.o \
rowfm1.o \
rowfm2.o \
runkut.o \
sandf.o \
sandq.o \
sandr.o \
save.o \
search.o \
seprt.o \
setup.o \
sfntr2.o \
sfntr3.o \
sfntrp.o \
shepard_norm.o \
shield.o \
shkexp.o \
simps1.o \
simpson.o \
skinfr.o \
smthna.o \
solvit.o \
sort.o \
sose.o \
sosec.o \
soset.o \
spec.o \
spfit.o \
spline.o \
spline2.o \
splinf.o \
```

```
      stag.o \
      stats3.o \
      strdat.o \
      stream.o \
      sum.o \
      surf.o \
      surf_int.o \
      surfcp.o \
      surfp.o \
      taper.o \
      tcalc.o \
      temp.o \
      trans.o \
      trim.o \
      turbln.o \
      ugas3.o \
      ugas4.o \
      valu2.o \
      valu3.o \
      value.o \
      viscus.o \
      vrtl.o \
      wderiv.o \
      wedge.o \
      wfltref.o \
      wgtavg.o \
      writms.o \
      writsc.o \
      wrtflo.o \
      wrtvisc.o \
      wshock.o \
      wsurf.o \
      zero.o


mk5: $(MOBJ)
      $(FOR) -o $@ $(MOBJ)
      mv $@ ../$@

geom.o:         geom.f comp.cmn
merid.o:  merid.f comp.cmn
monitr.o: monitr.f comp.cmn
mout.o:         mout.f comp.cmn
```

```
pres.o:         pres.f comp.cmn
presot.o: presot.f comp.cmn
sum.o:          sum.f comp.cmn
viscus.o: viscus.f comp.cmn
bl.o:           bl.f level2.cmn
blcf.o:         blcf.f level2.cmn
calc.o:         calc.f level2.cmn
cmpexp.o: cmpexp.f level2.cmn
expan.o:  expan.f level2.cmn
ffree.o:  ffree.f level2.cmn
getpdat.o:      getpdat.f level2.cmn
heat.o:         heat.f level2.cmn
idlgs.o:  idlgs.f level2.cmn
ledge.o:  ledge.f level2.cmn
modnew.o: modnew.f level2.cmn
nrml.o:         nrml.f level2.cmn
bl.o:           bl.f level2.cmn
blcf.o:         blcf.f level2.cmn
calc.o:         calc.f level2.cmn
cmpexp.o: cmpexp.f level2.cmn
expan.o:  expan.f   level2.cmn
ffree.o:  ffree.f level2.cmn
getpdat.o:      getpdat.f level2.cmn
heat.o:         heat.f level2.cmn
idlgs.o:  idlgs.f level2.cmn
ledge.o:  ledge.f level2.cmn
modnew.o: modnew.f level2.cmn
nrml.o:         nrml.f level2.cmn
obli01.o: obli01.f level2.cmn
oblidl.o: oblidl.f level2.cmn
obliqe.o: obliqe.f level2.cmn
oblrgs.o: oblrgs.f level2.cmn
obltbl.o: obltbl.f level2.cmn
plate.o:  plate.f level2.cmn
prop.o:         prop.f level2.cmn
rcstr.o:  rcstr.f level2.cmn
seprt.o:  seprt.f level2.cmn
setup.o:  setup.f level2.cmn
stag.o:         stag.f level2.cmn
strdat.o: strdat.f level2.cmn
surfp.o:  surfp.f level2.cmn
tcalc.o:  tcalc.f level2.cmn
trans.o:  trans.f level2.cmn
```

```
vrtl.o:         vrtl.f level2.cmn
wedge.o:  wedge.f level2.cmn


compile: $(MOBJ)

.f.o:
     $(RM) $@
     $(FOR) -c $(FFLAGS) $*.f
```

B.4 PrepMk5 Makefile

```
#
#  Makefile for PREPMK5 (S/HABP Mark 5 Text Pre-
Processor)
#

#
# set up logicals and flags for compile options
#

RM = rm -f
CC = cc
FOR = f77

CFLAGS    = -g
FFLAGS    = -g -C
DEFINES = -DSYSV
INCLUDES = -I/usr/include
LIBS =  -lX11 -lPW -lsun -lm
LIBS =  -lX11 -lPW -lm

#
# list files that comprise the PREPMK5 program
#

OBJ =     addext.o \
     aerocrd.o   \
     alfbet.o \
     auxi.o   \
     comorg.o \
     cut_plane.o \
     ellgen.o \
        ellipse.o \
     ffield.o   \
     fltcon.o \
     fsum.o   \
     geomio.o \
     hingel.o \
     icpcard.o \
     infcard.o \
     invisd.o \
     l2visc.o \
```

```
      panl_gen.o \
      panl_grp.o \
      pmcard.o \
      prepmk5.o \
      readin.o \
      readrl.o \
      readthree.o \
      rdline.o \
      refdim.o \
      sctran.o \
      sfelem.o \
      sfgeom.o \
      shieldc.o \
      specrd.o   \
      viscs.o \
      wrtcomp.o

#
# compile and link files as necessary
#

prepmk5: $(OBJ)
      $(FOR) -o $@ $(OBJ)

.f.o:
      $(RM) $@
      $(FOR) -c $(FFLAGS) $*.f
```

B.5 Plot Makefile

```
FOR      = f77
FFLAGS   =
CFLAGS   =
DEBUG    = -g
DEFINES  = -DSYSV

INCLUDES = -I/usr/include/X11
LIBS     =  -lX11 -lm
LDFLAGS  =
XOBJS    =
OBJS =    pluto.o graphic.o xplot.o datamenu.o
pscript.o plotmenu.o \
     fmain.o xdata.o      misc.o convert.o eqn.o
globals.o

# special stuff for some SUN systems
#INCLUDES = -I/usr/openwin/include

# special stuff for Hewlett Packard
#INCLUDES = -I/usr/include/X11R5  -
I/usr/include/Motif1.2
#LDFLAGS  = -L/usr/lib/X11R5 -L/usr/lib/Motif1.2
#FOR      = fort77
#XOBJS    = hp_getarg.o
#DEFINES  = -DSYSV -Dpluto_main_=pluto_main

../hplot: $(OBJS) $(XOBJS)
     rm -f $@
     $(FOR) -o $@ $(LDFLAGS) $(OBJS) $(XOBJS) $(LIBS)
.c.o:
     rm -f $@
     $(CC) -c $(CFLAGS) $(DEBUG) $(DEFINES) $(INCLUDES)
$*.c

.f.o:
     rm -f $@
     $(FOR) -c $(FFLAGS) $(DEBUG) $*.f

lint:   $(OBJS) $(XOBJS)
     lint $(INCLUDES) *.c > lint.out
```

B.6 Trim Makefile

```
RM  = rm -f
FOR = f77 -32
XOBJS    =

# special stuff for Hewlett Packard
#XOBJS   = hp_getarg.o

FFLAGS   =  -g -C

MOBJ =    get_inpt.o \
     polint.o \
     rdinput.o \
     rdline.o \
     read_habp.o \
     readin.o \
     readrl.o \
     rep_ext.o \
     trim.o \
     trimpost.o \
     wrtrim.o

trim:     $(MOBJ) $(XOBJS)
     $(RM) $@
     $(FOR) -o $@ $(MOBJ) $(XOBJS)
     mv trim ..

.f.o:
     $(RM) $@
     $(FOR) -c $(FFLAGS) $*.f
```

APPENDIX C

SPACE SHUTTLE ORBITER CENTER OF GRAVITY LOCATIONS

Table 7. Detailed Space Shuttle Orbiter Center of Gravity Locations (http://spaceflight.nasa.fov/shuttle/reference/green/massprop.pdf)

Miss. Seq. No.	STS-No.	Orb. OV-	Notes	Lift-off Weight, lb	CG X	Y	Z	Pre-Deorbit burn Weight, lb	CG X	Y	Z	Entry Interface Weight, lb	CG X	Y	Z	Mach 1 Weight, lb	CG X	Y	Z	Landing Weight, lb	CG X	Y	Z	Entry Weight, lb	CG X	Y	Z
1	1	102		219,440.7	1125.2	0.2	379.7	202,769.9	1108.4	0.1	376.1	196,868.7	1099	0.2	373.1	195,942.7	1096.7	0.2	372.4	195,472.7	1098.1	0.2	369.6	197,023.0	1120.7	0.3	371
2	2	102		230,938.9	1120.6	0.1	379.8	215,530.2	1106.1	0.3	377.1	206,842.5	1100.5	0.2	373.8	204,355.5	1096.6	0.2	372.3	204,262.5	1098.1	0.2	369.7	206,455.0	1116	0.1	372.7
3	3	102		235,556.1	1119.2	-0.5	379.4	214,949.6	1108.3	-0.5	376.1	208,790.2	1097.9	-0.5	373.3	207,349.2	1095.4	-0.5	372.4	207,072.9	1096.9	-0.5	369.8	211,200.0	1117.8	-0.4	373.5
4	4	102		241,772.0	1122.2	-0.3	381.8	218,163.6	1106.6	-0.5	377.7	211,184.0	1096.2	-0.5	374.5	209,140.5	1092.9	-0.5	373.3	208,946.8	1094.4	-0.5	370.7	214,526.0	1114.5	-0.4	375
5	5	102		247,112.9	1116.3	1.1	379.7	209,890.1	1105	1	374.5	203,775.9	1096.6	1	371.6	202,642.7	1094.8	1	371	202,480.3	1096.3	1	368.3	205,727.0	1118.4	1	371.9
6	6	099		256,928.1	1127.8	0.5	382.9	197,427.8	1111.2	0.3	374.6	191,384.2	1101.2	0.3	371.5	190,627.2	1099.7	0.4	370.9	190,330.2	1101.2	0.4	368	191,966.0	1131.4	0.4	371.9
7	7	099		249,362.7	1123.6	-0.2	381.2	211,737.0	1102	-0.6	376.5	204,983.4	1091.3	-0.6	373.3	204,340.4	1089.8	-0.6	372.8	204,043.4	1091.2	-0.6	370.1	204,576.0	1119.6	-0.6	373.6
8	8	099		242,912.3	1124.5	0.2	382	212,911.0	1098.2	-0.1	376.7	205,243.4	1092.5	-0.1	373.8	204,141.4	1090.4	-0.1	373	203,945.4	1091.9	-0.1	370.4	205,874.0	1119.4	-0.2	374.3
9	9	102		247,807.3	1109.7	-0.1	379	227,648.0	1097	0	378.6	221,143.4	1087.3	-0.1	373.7	220,288.4	1085.8	-0.1	373.2	220,027.4	1087.1	-0.1	370.7	219,910.0	1113.4	0	374.1
10	10	099	a	250,482.7	1124.5	0.2	381.5	209,746.1	1101.4	1.2	375.8	202,966.5	1090.7	1.3	372.6	201,528.5	1087.9	1.3	371.6	201,238.5	1089.3	1.3	368.8				
11	41C	099			1113.4	0.2	383.4	208,206.4	1117.4	-0.1	376.5	198,072.8	1101.8	-0.1	371.6	197,169.8	1100	-0.1	371	196,975.8	1101.6	-0.1	368.2	198,830.0	1130.9	-0.1	372.4
12	41D	103		263,477.4	1118	0	382.8	211,075.1	1100	-0.1	376.6	203,382.5	1093.4	-0.2	373.5	202,316.5	1090.7	-0.1	372.6	201,674.5	1091.7	-0.2	369.6	202,366.0	1121.8	-0.2	373.8

a = KSC landing
b = NA/DOD = Not Available/Department of Defense Mission
c = Vehicle destroyed at approximately 73 seconds
d = Computations not available

Source: JSC/VF Orbiter Mass Properties Summary, STS-1 and subsquent mission.

Table 7 (continued).

Miss. Seq. No.	STS-No.	Orb. OV-	Notes	Lift-off Weight, lb				Pre-Deorbit burn Weight, lb				Entry Interface Weight, lb				Mach 3 Weight, lb				Landing Weight, lb				Ferry Weight, lb			
				CG X	Y	Z		CG X	Y	Z		CG X	Y	Z		CG X	Y	Z		CG X	Y	Z		CG X	Y	Z	
13	41G	099	a	242,790.8				209,799.7				203,651.1				202,829.1				202,266.1							
				1119	-0.1	381.7		1093.5	-0.2	374.6		1085.4	-0.2	371.9		1083.7	-0.2	371.3		1084.8	-0.1	368.4					
14	51A	103	a	263,324.6				215,715.3				209,163.7				207,982.7				207,505.7							
				1120.9	-0.1	382.6		1090.2	-0.2	375.2		1083.4	-0.2	372.5		1081.4	-0.2	371.8		1082.6	-0.1	369.1					
15	51C	103	a,b																								
16	51D	103	a	250,891.6				209,102.8				199,742.2				198,167.2				198,014.2							
				1126.5	-0.1	381.7		1110.6	-0.2	377		1095.6	-0.1	372.5		1092.7	-0.1	371.3		1094.3	-0.1	368.6					
17	51B	099		247,291.3				228,859.0				214,787.4				213,795.4				213,499.4				213,363.0			
				1114.2	-0.2	381.4		1096.7	-0.3	378		1085.7	-0.3	373.4		1084.1	-0.3	372.8		1085.4	-0.3	370.3		1114.8	-0.2	373.8	
18	51G	103		258,421.9				213,105.0				205,624.4				204,321.4				204,169.4				204,387.0			
				1109.6	0.2	379.6		1091.5	-0.2	375.2		1084.3	0	372.2		1082.1	0	371.4		1083.7	0	368.8		1114.2	0	372.9	
19	51F	099		252,628.9				225,398.0				218,227.4				216,894.4				216,735.4				217,564.7			
				1111.6	-0.4	381.8		1091.1	-0.5	376.3		1082.3	-0.6	373.4		1079.8	-0.6	372.5		1081.3	-0.6	370		1109.5	-0.5	373.9	
20	51I	103		262,309.7				207,794.8				197,824.4				196,856.4				196,674.4				197,259.3			
				1121.3	0.5	382.5		1110	0.2	376.7		1094.4	0.2	371.9		1092.4	0.3	371.3		1094.2	0.3	368.5		1124.9	0.3	372.7	
21	51J	104	b																					191,623.0			
22	61A	099		243,762.5				223,317.8				215,255.4				214,325.4				214,171.4				214,138.3			
				1109	-0.1	380.4		1091.8	-0.4	377.1		1085.5	-0.4	374.2		1083.8	-0.4	373.6		1085.2	-0.4	371.1		1116.4	-0.3	374.5	
23	61B	104		261,610.1				213,335.8				206,187.4				205,880.4				205,732.4				205,682.3			
				1110.3	0	379.3		1096.9	-0.1	375.3		1085.8	-0.2	372		1084.4	-0.1	371.5		1085.9	-0.1	368.9		1118	-0.1	373.2	
24	61C	102		258,003.0				221,485.8				211,194.4				210,325.4				210,181.4				210,430.0			
				1110.3	0.4	380.3		1098.1	0.4	375.7		1085.2	0.4	371.4		1083.6	0.4	370.9		1085.1	0.4	368.3		1114.9	0.5	373.2	

a = KSC landing
b = NA/DOD = Not Available/Department of Defense Mission
c = Vehicle destroyed at approximately 73 seconds
d = Computations not available

Source: JSC/VF Orbiter Mass Properties Summary, STS-1 and subsequent mission.

Table 7 (continued).

Miss. Seq. No.	STS-No.	Orb. OV-	Notes	Lift-off Weight, lb CG X	Y	Z	Pre-Deorbit burn Weight, lb CG X	Y	Z	Entry Interface Weight, lb CG X	Y	Z	Mach 3 Weight, lb CG X	Y	Z	Landing Weight, lb CG X	Y	Z	Ferry Weight, lb CG X	Y	Z
25	51L	099	c	268,829.6																	
				1119.1	-0.2	384															
26	26	103		254,606.5			202,676.3			194,985.3			194,347.3			194,184.3			193,936.0		
				1118.4	0.3	380.6	1104.7	0.1	374.6	1097.9	0.2	371.4	1096.6	0.2	371	1096.3	0.2	368.2	1131.8	-0.1	372
27	27	104	b				200,752.5			192,095.3			191,105.3			190,956.3			191,337.7		
							1107.9	-0.9	374.6	1095.2	-0.9	370.3	1093.4	-0.9	369.7	1095.1	-0.9	366.8	1127.1	-0.9	370.8
28	29	103		256,357.6			202,517.6			195,531.6			194,939.6			194,789.6			194,710.0		
				1116.4	0.6	380.8	1104.1	0.5	374.6	1095.1	0.5	371.4	1093.7	0.5	370.9	1095.3	0.5	368.1	1128.6	0.3	372
29	30	104		261,118.9			201,074.6			193,349.6			192,557.6			192,459.6			193,031.0		
				1123.4	0.5	382.6	1106.8	0.4	374.5	1098.7	0.4	371.1	1097.3	0.4	370.6	1099.1	0.4	367.8	1130.7	0.2	371.7
30	28	102	b				207,482.2			201,294.2			200,331.2			200,214.2			200,509.7		
							1096.7	-0.1	373.1	1089.7	-0.1	370.4	1087.8	-0.1	369.7	1089.4	-0.1	367	1120.5	-0.2	370.8
31	34	104		257,569.2			204,439.2			196,784.2			196,112.2			195,954.2			195,804.0		
				1114.2	0.4	380.8	1101.8	0.2	375	1094.5	0.3	371.7	1093.1	0.2	371.2	1094.7	0.3	368.5	1128.2	0.1	372.3
32	33	103	b				203,006.2			195,185.2			194,463.2			194,282.2			195,242.7		
							1106.2	0	375.1	1094.1	0.1	371.1	1093.2	0.1	370.8	1094.8	0.1	368	1124.7	0.1	371.8
33	32	102		255,994.0			241,970.2			229,892.2			228,523.2			228,335.2			227,868.7		
				1131.3	-0.9	381.4	1096.3	-0.9	378.6	1080.8	-0.9	373.8	1078.2	-0.9	372.9	1079.6	-0.9	370.5	1108.8	-0.8	373.8
34	36	104	b				193,208.2			188,059.2			187,316.2			187,200.2			187,944.7		
							1105.2	0.1	373.1	1096.2	0.2	370.4	1094.7	0.2	369.8	1096.4	0.2	366.9	1128.9	0.1	370.8
35	31	103		249,109.2			202,753.2			190,566.2			189,309.2			189,118.2			189,691.7		
				1114.8	-0.5	384.2	1107.2	-1	376.4	1090	-1	370.5	1087.9	-1	369.7	1089.7	-1	366.6	1125.1	-1	370.3
36	41	103		259,593.9			204,007.2			197,986.2			196,982.2			196,869.2			197,369.7		
				1115.2	-0.1	381.4	1100.4	-0.5	374.7	1090.4	-0.5	371.8	1089.4	-0.4	371.2	1091.2	-0.4	368.3	1124.4	-0.5	372

a = KSC landing
b = NA/DOD = Not Available/Department of Defense Mission
c = Vehicle destroyed at approximately 73 seconds
d = Computations not available

Source: JSC/VF Orbiter Mass Properties Summary, STS-1 and subsequent mission.

Table 7 (continued).

Miss. Seq. No.	STS-No.	Orb. OV-	Notes	Lift-off Weight, lb			Pre-Deorbit burn Weight, lb			Entry Interface Weight, lb			Mach 3 Weight, lb			Landing Weight, lb			Ferry Weight, lb		
				CG X	Y	Z	CG X	Y	Z	CG X	Y	Z	CG X	Y	Z	CG X	Y	Z	CG X	Y	Z
37	38	104	a				196,781.2			191,862.2			191,409.2			191,091.2					
							1106.3	0.2	372.8	1098.1	0.2	370.3	1096.2	0.2	369.9	1096.6	0.2	366.7			
38	35	102		256,385.6			236,566.2			226,613.2			225,531.2			225,329.2			223,330.7		
				1106.4	-0.5	378.1	1092.5	-0.5	375.4	1080.8	-0.5	371.4	1079.1	-0.5	370.8	1080.5	-0.4	368.4	1114.7	-0.3	371.6
39	37	104		255,824.0			201,055.2			191,569.2			190,266.2			190,098.2			190,023.7		
				1116.5	-0.3	381.7	1103	-0.6	375.4	1089.6	-0.6	370.9	1087.4	-0.6	370	1089.2	-0.6	367	1124.2	-0.6	370.6
40	39	103	a	247,373.4			218,919.2			212,806.2			211,673.2			211,512.2					
				1111.1	0	382.5	1091	-0.4	376.8	1082.2	-0.3	374.1	1080.3	-0.4	373.5	1082	-0.4	370.8			
41	40	102		251,970.3			235,196.2			227,709.2			226,737.2			228,535.2			225,326.7		
				1100.2	-0.1	378.4	1089.5	-0.2	374.9	1081.1	-0.2	371.9	1079.6	-0.2	371.4	1080.9	-0.2	369	1112.9	-0.1	372.2
42	43	104	a	259,374.7			203,898.2			197,472.2			196,353.2			196,088.5					
				1113.9	-0.2	380.4	1099.5	-0.3	374.2	1088.8	-0.3	371	1087.4	-0.3	370.3	1089.7	-0.3	367.3			
43	48	103		240,062.6			204,685.2			193,665.2			192,925.2			192,780.2			193,583.7		
				1125.5	-0.9	381.9	1113.1	-0.9	375.9	1097.4	-1	370.6	1098	-1	370	1097.8	-0.9	367	1130.2	-0.9	371.3
44	44	104		259,904.0			204,165.2			196,229.2			195,047.2			194,818.2			194,087.1		
				1118.2	0	381	1102.6	-0.2	374.4	1092.4	-0.2	370.7	1090.8	-0.2	370	1092.5	-0.2	367	1128.6	-0.1	371.1
45	42	103		243,494.1			227,227.2			219,459.2			218,159.2			218,089.2			218,224.7		
				1104.8	-0.1	376.3	1091.4	-0.3	376.6	1082.3	-0.3	373.4	1080.6	-0.3	372.8	1082.2	-0.3	370.1	1115.6	-0.2	373.1
46	45	104	a	233,652.0			215,275.2			208,495.2			205,672.3			205,588.2					
				1113.1	-0.3	377.6	1100.3	-0.5	375.2	1086.3	-0.5	371	1085.4	-0.4	370.5	1087.2	-0.4	367.7			
47	49	105		258,392.3			209,002.2			202,094.2			201,400.2			201,235.2			199,831.2		
				1119.5	-0.3	383.9	1096.7	-0.6	375	1085.8	-0.7	371.7	1084.4	-0.6	371.2	1086.2	-0.6	368.3	1122.7	-0.5	371.9
48	50	102	a	257,338.6			236,634.2			227,587.2			225,865.2			225,815.2					
				1108	-0.5	378.8	1089.7	-0.6	375.9	1079.8	-0.7	372.4	1107.7	-0.7	371.6	1079.1	-0.7	369			

a = KSC landing
b = NA/DOD = Not Available/Department of Defense Mission
c = Vehicle destroyed at approximately 73 seconds
d = Computations not available

Source: JSC/VF Orbiter Mass Properties Summary, STS-1 and subsequent mission.

Table 7 (continued).

Miss. Seq. No.	STS-No.	Orb. OV-	Notes	Lift off Weight, lb				Pre Deorbit burn Weight, lb				Entry Interface Weight, lb				Mach 3 Weight, lb				Landing Weight, lb				Ferry Weight, lb			
				CG X	Y	Z		CG X	Y	Z		CG X	Y	Z		CG X	Y	Z		CG X	Y	Z		CG X	Y	Z	
49	46	104	a	256,026.3				216,581.2				210,995.2				209,851.2											
				1113.8	-0.3	382.4		1087.1	-0.5	374.8		1080.2	-0.5	372.4		1078.2	-0.5	371.7		1079.6	0.5	368.9					
50	47	105	a	244,645.2				228,709.2				221,374.2				220,325.2				220,195.2							
				1103.9	-0.4	379.1		1091.1	-0.5	377.5		1085.4	-0.5	374.9		1083.7	0.5	374.3		1085.3	-0.5	371.7					
51	52	102	a	250,399.4				223,297.2				217,359.2								215,979.2							
				1109.5	-0.3	377.5		1090.3	-0.4	373.5		1084.5	-0.4	371.1		1082.6	-0.4	370.4		1084.3	-0.3	367.7					
52	53	103		243,944.4				201,376.2				194,826.2				194,028.2				193,851.2				193,648.3			
				1112.3	0.1	380.7		1100.2	0	373.9		1090.4	0.1	370.5		1089.5	0	370.2		1091.3	0.1	367.1		1125.3	0.2	370.8	
53	54	105	a	259,764.2				205,293.6				198,296.6				197,481.2				197,353.2							
				1115.7	0.3	381.2		1101.4	0.2	375		1093.5	0.2	371.9		1091.6	0.2	371.3		1093.4	0.2	368.4					
54	56	103	a	237,213.0				217,922.2				209,229.2				208,052.2				207,946.2							
				1109.5	-0.3	379.3		1098.3	-0.5	376.9		1086.3	-0.5	373.4		1084.6	-0.4	372.5		1086.3	-0.4	369.7					
55	55	105		255,441.8				236,094.2				228,546.6				227,484.2				227,209.2				226,360.2			
				1101.6	-0.6	377.5		1089	-0.6	375.4		1080.1	-0.6	372.4		1078.4	-0.6	371.9		1079.7	-0.6	369.2		1111.8	-0.5	372.3	
56	57	105	a,d	252,710.1								226,573.5				225,019.5				224,906.5							
				1112.6	-0.1	382.9						1083	-0.2	375.2		1080.9	-0.2	374.6		1082.5	-0.2	372					
57	51	103	a,d	261,486.6								208,048.5				207,042.5				206,931.5							
				1116.5	-0.6	381.5						1086.6	-0.8	373.5		1084.7	-0.7	373.1		1086.5	-0.7	370.3					
58	58	102	d	256,097.0								230,447.7				229,480.7				229,368.7				229,953.7			
				1103.4	-0.4	378						1080	-0.5	373		1078.8	-0.5	372.7		1080.4	-0.5	370.2		1107.9	-0.6	373.7	
59	61	105	a,d	250,279.1								213,640.5				212,946.5				212,835.5							
				1113.5	-0.1	381.6						1080.2	0	372.2		1078.8	0.1	371.9		1080.5	0.07	369.2					
60	60	103	a,d	245,767.5								217,583.5				216,662.5				216,594.5							
				1104.8	-0.7	380.2						1081.2	-0.9	374.1		1079.6	-0.9	373.7		1081.3	-0.9	371.1					

a = KSC landing
b = NA/DOD = Not Available/Department of Defense Mission
c = Vehicle destroyed at approximately 73 seconds
d = Computations not available

Source: JSC/VF Orbiter Mass Properties Summary, STS-1 and subsequent mission.

Table 7 (continued).

Miss. Seq. No.	STS-No.	Orb. OV-	Notes	Lift-off Weight, lb				Pre-Deorbit burn Weight, lb				Entry Interface Weight, lb				Mach 3 Weight, lb				Landing Weight, lb				Ferry Weight, lb			
				CG X	Y	Z		CG X	Y	Z		CG X	Y	Z		CG X	Y	Z		CG X	Y	Z		CG X	Y	Z	
61	62	102	a,d	256,584.1								229,091.2				228,360.2				228,250.2							
				1107.4	-0.6	379.2						1084	-0.7	373.5		1182.6	-0.6	373.2		1084.1	-0.6	370.6					
62	59	105	d	246,851.0								222,698.0				221,931.0				221,865.0				222,734.0			
				1095.8	-0.5	378.7						1090.9	-0.4	374.7		1079.6	-0.4	374.5		1081.2	-0.4	371.9		1109.1	-0.6	375.5	
63	65	102	a	258,585.0				237,613.0				230,624.0				229,410.0				229,307.0							
				1104.2	-0.2	378.8		1087.4	-0.6	375.6		1080.7	-0.6	373		1079	-0.6	373		1080.1	-0.6	370					
64	64	103		240,864.0				221,336.0				213,510.0				212,565.0				212,141.0				212,251.0			
				1105.5	-0.5	379.5		1090.1	-0.7	376.8		1083.7	-0.8	373.5		1082	-0.8	373.1		1083.9	-0.7	370.4		1117.1	-0.5	373.8	
65	68	105		247,136.0				228,874.0				222,752.0				221,460.0				221,571.0				221,390.0			
				1099.1	-0.5	378.5		1087.8	-0.4	376.8		1080.1	-0.4	374.3		1078.1	-0.4	373.7		1080.3	-0.4	371.4		1112.2	-0.4	374.6	
66	66	104		243,069.0				221,520.0				212,378.0				211,434.0				211,327.0				210,966.0			
				1113	-0.1	379.5		1096.8	-0.1	375.9		1085.9	-0.1	371.9		1084.3	-0.1	371.6		1086	-0.1	368.9		1120.1	0	372.4	
67	63	103	a	247,555.0				224,130.0				213,717.0				212,772.0				212,646.0							
				1111.1	-0.2	382.2		1095.7	-0.5	378.4		1081.4	-0.6	373.9		1079.7	-0.5	373.5		1079.3	-0.5	373.6					
68	67	105		256,293.0				231,034.0				218,563.0				217,568.0				217,481.0				216,663.0			
				1118	0	381.5		1101.4	0	377.5		1084.1	0	372		1082.5	0	371.6		1083.1	0	371.9		1117.9	0	372.9	
69	71	104	a	248,856.8				227,051.7				217,202.0				215,036.6				214,879.4							
				1110.1	-0.3	380.4		1094.1	-0.2	377.1		1081.9	-0.2	372.4		1080.1	0	372.1		1081	-0.2	369.4					
70	70	103	a	258,798.0				205,887.5				197,482.7				196,725.9				196,574.8							
				1120.2	0.1	380.6		1106.6	0.1	375.1		1099	0.1	371.5		1097.6	-0.1	371.2		1099.4	0.1	368.2					
71	69	105	a	258,644.9				229,422.3				220,383.0				219,494.4				219,377.0							
				1112.6	0.2	383.3		1092.9	0.4	378.4		1082.2	0.05	374.7		1080.5	0.4	374.3		1081.3	0.4	371.6					
72	73	102	a	257,017.5				239,035.7				231,578.0				230,621.7				230,469.3							
				1101.3	-0.6	377.2		1089.3	-0.5	375.8		1081.9	-0.5	372.9		1080.5	-0.5	372.6		1082	-0.5	370					

a = KSC landing
b = NA/DOD = Not Available/Department of Defense Mission
c = Vehicle destroyed at approximately 73 seconds
d = Computations not available

Source: JSC/VF Orbiter Mass Properties Summary, STS-1 and subsquent mission.

Table 7 (continued).

Miss. Seq No.	STS-No.	Orb. OV-	Notes	Lift-off Weight, lb				Pre-Deorbit burn Weight, lb				Entry Interface Weight, lb				Mach 3 Weight, lb				Landing Weight, lb				Ferry Weight, lb			
				CG X	Y	Z		CG X	Y	Z		CG X	Y	Z		CG X	Y	Z		CG X	Y	Z		CG X	Y	Z	
73	74	104	a	274,560 2				215,856 9				204,058 7				203,101 9				202,950.9							
				1113	0 1	381 7		1113 4	0.7	370 4		1080 8	0 2	371 5		1078 8	0 2	371		1080 5	0 2	368 2					
74	72	105	a	247,320 5				226,239.4				218,151 1				217,394 2				217,243 4							
				1117 6	-0.1	381.7		1090 5	0	376 2		1081 9	0	372.9		1080 6	0	372 6		1082 2	0 1	369 9					
75	75	102	a	261,250 1				240,782.4				229,357 8				228,601.1				228,449.9							
				1106	-0 4	379.9		1092.6	-0 3	377 5		1079.7	-0 3	373		1078 4	-0 3	372.7		1079.9	-0 3	370 2					
78	76	104		246,337.3				220,475.9				211,094 8				210,143 0				209,993.4				210,600.3			
				1109 7	-0 2	379.7		1095 8	0	375.8		1083.4	0	371 6		1081.7	0	371.2		1083 3	0	368 4		1113.5	-0 1	372 4	
77	77	105	a	254,890.5				233,219 3				222,936 2				221,979 5				221,828.4							
				1106.4	-0.1	380 4		1094.6	-0 1	377.6		1081.8	-0 1	373 4		1080.3	-0.1	373		1081.8	-0.1	370.4					
78	76	102	a	258,144 6				238,077.2				229,652.9				228,696 3				228,545.4							
				1102.7	-0.4	377.2		1088.9	-0.2	375.6		1081 9	-0 2	372.5		1080.5	-0 2	372.1		1082	-0 2	369 5					
79	79	104	a	249,327 5				225,654 4				216,359.8				215,177.8				215,026.5							
				1109 2	0	379.8		1094.2	0.1	378		1081 2	0.1	371 9		1079 4	0.1	371.4		1081	0 2	368.7					
80	80	102	a	260,935 2				238,607.0				226,516 3				227,534 4				227,383.2							
				1106.5	-0.3	381		1091.2	-0.4	377.7		1080 2	-0.4	373 8		1078.4	-0 4	373.4		1079.9	-0 4	370.9					
81	81	104	a	249,935 7				225,432 8				218,042.8				214,861.6				214,710.6							
				1110.7	0	379 8		1079.1	0 2	376.1		1082.7	0.3	371.8		1080.6	0.3	371.3		1082 5	0.3	368.6					
82	82	103	a	251,238.1				221,530.0				214,393 2				213,636 6				213,485 7							
				1112.8	-0.1	381.2		1087.2	0.1	374.6		1079.2	0 1	371 6		1077.9	0.1	371 3		1079 5	0.1	368 5					
83	83	102	a,d	259,143.6				240,257.2				231,584.3				230,507.6				230,276 3							
				1102.1	-0.3	378 2		1088.5	-0 2	376.8		1081.7	-0 2	373.7		1079 9	-0.2	373 3		1081.3	-0 2	370.5					
84	84	104	a	249,462.2				224,584.2				214,653.8				213,697.9				213,547 2							
				1109.1	0.1	379.7		1094.6	0 3	375.9		1080	0.3	371.4		1078.4	0.3	371		1080	0 4	368 3					

a = KSC landing
b = NA/DOD = Not Available/Department of Defense Mission
c = Vehicle destroyed at approximately 73 seconds
d = Computations not available

Source: JSC/VF Orbiter Mass Properties Summary, STS-1 and subsquent mission.

Table 7 (continued).

	Miss Seq No.	STS-No	Orb. OV-	Notes	Lift-off Weight, lb			Pre Deorbit burn Weight, lb			Entry Interface Weight, lb			Mach 3 Weight, lb			Landing Weight, lb			Ferry Weight, lb		
					CG X	Y	Z	CG X	Y	Z	CG X	Y	Z	CG X	Y	Z	CG X	Y	Z	CG X	Y	Z
1	85	94	102	a	260,248.6			240,407.8			231,591.0			230,514.5			230,283.5					
					1102.1	-0.2	378.1	1088.6	-0.2	376.3	1080.2	-0.3	373	1079.6	-0.3	372.6	1080	-0.2	370.1			
1	86	85	103	a	249,695.6			228,129.5			220,185.2			219,228.6			219,077.0					
					1102.7	0	379.5	1088.5	0.1	376.8	1079.9	0.1	373.6	1078.4	0.1	373.2	1079.9	0.1	370.6			
1	87	86	104	a	252,035.4			225,501.0			215,616.7			214,660.0			214,509.0					
					1109.8	0.3	379.8	1094.5	0.3	376.1	1080.6	0.3	371.3	1079	0.3	371.3	1080.6	0.3	368.5			

a = KSC landing
b = NA/DOD = Not Available/Department of Defense Mission
c = Vehicle destroyed at approximately 73 seconds
d = Computations not available

Source JSC/VF Orbiter Mass Properties Summary, STS-1 and subsquent mission.

APPENDIX D

STANDARD ATMOSPHERIC PROPERTIES

Information for the atmospheric properties was taken from the U.S. Standard Atmosphere, 1976. All properties were taken at an altitude of 160 kilometers.

From Table I, pg 69,

Temperature: 696.29 K

From Table II, pg 93,

Number density: 3.162 (10^{16}) m^{-3}

Mean free path: 53 meters

Molecular Weight: 23.49 kg/kmol

From Table VIII, pg 211,

Atmospheric Composition Number Density:

Nitrogen (N_2): 1.774 (10^{16}) m^{-3}

Atomic Oxygen (O): 1.238 (10^{16}) m^{-3}

Oxygen (O_2): 1.460 (10^{15}) m^{-3}

Argon (Ar): 2.321 (10^{13}) m^{-3}

Helium (He): 1.861 (10^{13}) m^{-3}

Hydrogen (H): 2.911 (10^{11}) m^{-3}

VITA

Nadine Lashier was born in Silver Spring, Maryland, in 1975. She attended high school at Bass Memorial Academy in Lumberton, Mississippi, graduating in May 1993. She received a Bachelor of Science in Engineering Degree in Mechanical Engineering from Walla Walla College, located in College Place, Washington, in June 1997. In August of 1997, she began classes at the University of Tennessee Space Institute, in Tullahoma, Tennessee. She was awarded a Master of Science Degree in Aerospace Engineering from the University of Tennessee, Knoxville, in May 1999.